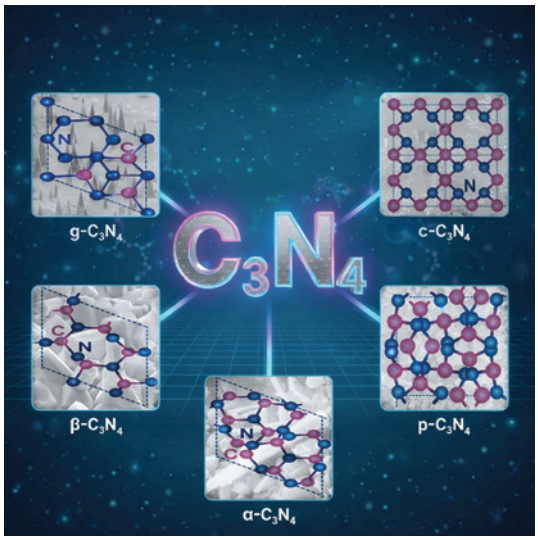
https://doi.org/10.59761/RCR5243

Carbon nitride polymorphs: materials of the future

Anna V. Khlyustova,[a]* Xianqiang Xiong,[b] Valeriya D. Aisina,[a] Nikolay A. Sirotkin,[a] Aleksandra D. Radina,[c] Alexander G. Kvashnin,[c] Kangle Lv,[d] Alexander V. Agafonov[a]

[a] *G.A.Krestov Institute of Solution Chemistry, Russian Academy of Sciences, 153012 Ivanovo, Russian Federation*
[b] *School of Pharmaceutical and Chemical Engineering, Taizhou University, 318000 Jiaojiang, China*
[c] *Skolkovo Institute of Science and Technology, 121205 Moscow, Russian Federation*
[d] *College of Resources and Environment, South-Central Minzu University, 430074 Wuhan, China*



The search for non-metal photocatalysts is of considerable scientific and practical interest due to the growing environmental concerns associated with photocatalysis. Among such materials, graphitic carbon nitride (g-C_3N_4) undoubtedly holds the highest priority. The focus on this material has diverted the attention of researchers away from other polymorphs of carbon nitrides, the solid phases of which, namely α, β, cubic, and pseudocubic phases, behave similarly to diamond-like structures (diamond, silicon nitrides, boron nitrides). These phases have a significant potential due to their structural features in both a pure state and composites. Although research into carbon nitride started with attempts to obtain dense carbon nitride phases and theoretically investigate them, these phases are currently the least explored in terms of their practical applicability. These issues are addressed in only a few studies. The main challenge here lies in creating the special conditions required for the formation of dense phases. This review critically examines the structure, synthesis methods, product yields, and morphology of both dense and layered polymorphs of carbon nitride. The evolution of synthetic approaches to dense carbon nitride polymorphs is demonstrated, and the results of theoretical studies on the band structure are analysed, along with the approximations used. This review consolidates fragmented data on various C_3N_4 polymorphs, highlighting the diversity of factors that influence their structure and morphology. Data on potential uses for dense carbon nitride phases, including their composites as photocatalysts, are also presented.
The bibliography includes 144 references.
Keywords: carbon nitride, dense polymorph, morphology, DFT, photocatalyst.

Contents

1. Introduction 1
2. Polymorphs 3
2.1. Structure 3
2.2. Identification 4
3. Properties of polymorphs 5
3.1. Physical characteristics 5
3.2. Optical properties 5
4. Preparation methods 7
5. Morphology of polymorph particles 10
6. Potential applications of carbon nitride 12
6.1. Wear-resistant coatings 12
6.2. Photocatalysts 13
6.2.1. Removal of dyes 13
6.2.2. Water splitting 14
6.3. Optoelectronics and sensor technology 15
7. Conclusion 15
8. List of abbreviations and symbols 16
9. References 16

1. Introduction

After a publication by Fujishima and Honda[1] devoted to electrochemical photolysis of water using titanium dioxide, TiO_2 became the most actively studied photocatalyst. To date, approximately 100 thousand scientific papers have been devoted to photocatalysis using TiO_2, which is the gold standard of photocatalytic processes due to its low cost, lack of toxicity and chemical stability. However, the early 21st century saw the discovery of new photocatalytically active materials, which began to compete with titanium dioxide. The main disadvantage of TiO_2 is its wide band gap (~3.2 eV for anatase), which limits its activity to the ultraviolet range (less than 5% of sunlight), and therefore, the search for effective photocatalysts in the visible range has become a priority.

Materials based on compounds of carbon and nitrogen, particularly polymorphs with the general formula C_3N_4, have been the focus of attention of materials scientists, chemists and physicists for several decades. This interest, which originated from theoretical calculations, has developed into a broad and dynamic field of research with real industrial applications. Currently, attention is focused on graphitic carbon nitride

Received 15 May 2026
© 2026 Uspekhi Khimii, ZIOC RAS, Russian Academy of Sciences

(g-C_3N_4), which has become a key material for photocatalysis and green chemistry. Interest in carbon nitrides has experienced a real boom since 2009. According to various estimates, approximately 45–50 thousand scientific papers were published over less than 20 years.[2–6] Other, more exotic C_3N_4 polymorphs continue to attract attention despite the enormous difficulty of their synthesis as alternative materials for wear-resistant coatings due to their unique, and sometimes record-breaking properties such as density (ρ), bulk modulus (*B*), and thermal conductivity coefficient (Table 1).

Carbon nitride C_3N_4 is a classic example of polymorphism, where the same chemical compound crystallizes as different structural forms with significantly different properties. This is due to the ability of carbon and nitrogen atoms to exist in different hybridization states (sp, sp^2, sp^3), which allows for the formation of both a layered graphite phase with extensive surface area (g-C_3N_4) and dense three-dimensional structures (β-, cubic) with exceptional mechanical strength (451–496 GPa). Understanding the relationship between synthesis conditions, structure, and functional properties of materials is essential for targeted design of C_3N_4-based materials with specified characteristics to solve specific problems in the fields of hydrogen energy production, photocatalysis, and purification of gases and liquids.

The existence of the carbon and nitrogen material β-C_3N_4 featuring short covalent bonds and sp^3 hybridization of carbon atoms was first theoretically predicted.[11] According to calculations, the tetrahedral geometry with C–N bond lengths in the range of 1.47–1.49 Å range may provide bulk modulus of 461–483 GPa, which is far superior to that of diamond. This prediction sparked a real gold rush for the search for superhard materials capable of replacing diamond, especially for high-temperature applications where carbon is oxidized.

Table 1. Mechanical properties of selected solid materials.

Material	*B*, GPa	*ρ*, g·cm^{-3}	Thermal conductivity coefficient, W m^{-1} K^{-1}	Refs
Diamond	443	3.5	2500	7
BN	369	2.18	400	8
$A^{III}B^{V}$ [a]	40–80	4.8–6.2	45–200	9
α-C_3N_4	351	3.45		10
β-C_3N_4	451	3.45	1200 [b]	10
c-C_3N_4	496	3.89		10
p-C_3N_4	448	3.81		10

[a] Chemical compounds consisting of Group III and V elements of the Periodic Table. [b] Calculated value.

The first works on the synthesis and study of the properties of C_3N_4 polymorphs focused on the development of synthetic protocols and the prediction of the properties of these materials. These include the following solid phases: α-C_3N_4 (analogous to α-Si_3N_4), β-C_3N_4, cubic c-C_3N_4 (with a zinc blende structure), and pseudocubic p-C_3N_4.[10–20] In addition to their potential superhardness, these phases are expected to have high thermal conductivity (1200 W m^{-1} K^{-1}), chemical inertness, and wide band gaps (4–6 eV). By analogy with semiconductors, carbon nitride was considered to be a promising material for high-temperature and high-frequency electronics and for protective optical coatings.

According to calculations,[10,11,13] at high pressures, α-C_3N_4 and g-C_3N_4 should be energetically more favourable than β-C_3N_4. Theoretical studies using density functional theory (DFT) have predicted the possible existence of λ-C_3N_4, cubic γ-C_3N_4, tetragonal t-C_3N_4, and monoclinic m-C_3N_4. It is noteworthy that the synthesis of well-crystallized α- or β-phases of C_3N_4 proved to be incredibly challenging. The proposed methods (magnetron sputtering, laser ablation, chemical vapour deposition, high-pressure methods) resulted in the formation of amorphous or nanocrystalline films with high density of defects or contaminated products. There were no practical methods for preparing these polymorphs in significant amounts or their real applications.

Therefore, g-C_3N_4 obtained from readily available large-scale raw materials (melamine, urea, cyanurates, *etc*.) through direct polycondensation at temperatures of 500–600°C, which was unexpectedly found to be an organic polymeric semiconductor with a band gap of about 2.7 eV, *i.e*., it actively absorbed visible light, and to be nontoxic and highly chemically and thermally stable (up to ~600°C in air).[21] These properties have attracted considerable attention for the potential use of g-C_3N_4 as a promising material for the development of photocatalysts active in the visible spectral range.

To date, a number of review papers have been published on various aspects of the chemistry and physics of carbon nitride have been published.[2–6] A significant portion of these studies is focused only on the graphitic g-C_3N_4 phase, including its photocatalytic application, in particular for water splitting, CO_2 reduction, and degradation of organic pollutants. Some reviews

A.**V**.**Khlyustova**. Candidate of Chemical Sciences, Senior Researcher.
E-mail: kav@isc-ras.ru
Current research interests: electrical discharge in liquids, transport processes, reactive species, material modification.
X.**Xiong**. PhD, Associate Professor.
E-mail: 11337061@zju.edu.cn
Current research interests: photocatalytic and photoelectrochemical materials, particularly heterojunctions, defect-engineered semiconductors.
V.**D**.**Aisina**. Candidate of Chemical Sciences, Junior Researcher.
E-mail: leric2009@yandex.ru
Current research interests: hybrid nanomaterials, functional materials, supramolecular systems, oxide structures, photocatalysts.
N.**A**.**Sirotkin**. Candidate of Chemical Sciences, Researcher.
E-mail: Alexsad8@yandex.ru
Current research interests: in-liquid plasma, synthesis of nanostructures, transport processes.
A.**D**.**Radina**. Post-graduate student, research assistant.
E-mail: Aleksandra.Radina@skoltech.ru
Current research interests: DFT simulation, electronic structure, two-dimensional materials, superhard materials.
A.**G**.**Kvashnin**. Doctor of Physical and Mathematical Sciences, Professor.
E-mail: A.Kvashnin@skoltech.ru
Current research interests: DFT simulation, electronic structure, two-dimensional materials, superhard materials, catalysis.
K.**Lv**. PhD, Professor.
E-mail: lvkangle@mail.scuec.edu.cn
Current research interests: photocatalytic nanomaterials, g-C_3N_4-based heterojunctions, defect-engineered semiconductors.
A.**V**.**Agafonov**. Doctor of Chemical Sciences, Professor, Head of Research Department.
E-mail: ava@isc-ras.ru
Current research interests: development of new materials, self-assembly and self-organization principles, hybrid organic-inorganic nanocomposites.
Translation: Z.P.Svitanko

also consider doping methods, the design of heterostructures, and defect engineering of g-C_3N_4 in order to enhance photocatalytic activity. Meanwhile, dense polymorphs (α-, β-, cubic, pseudocubic) are fragmentarily considered in the review literature, either in the context of historical attempts to synthesize superhard materials [10,11] or as a brief mention of the structural diversity of C_3N_4, without systematic analysis of preparation methods, synthesis conditions, phase purity, and correlations with functional properties. Furthermore, the existing reviews virtually lack a critical analysis of the methods for phase identification of dense phases and a comparison of the scattered data concerning their band structure and morphology. Therefore, there are still unresolved questions about how accurately various polymorphs can be identified, what synthesis methods actually produce single-phase samples, and how structural features affect electronic properties and photocatalytic activity.

This review aims to fill the gaps mentioned above. The review is not solely focused on one polymorph or its composites, but gives a systematic analysis of all experimentally obtained dense phases and methods for their synthesis. Scattered data on different forms of carbon nitride are integrated. Since carbon nitride has various potential applications (photocatalysis, hydrogen energy, protective coatings), it is important to demonstrate the diversity of factors that determine the structure and surface morphology.

2. Polymorphs

2.1. Structure

The polymorph g-C_3N_4 is called graphitic carbon nitride, because of the graphite sheets arranged along the *c* axis. Teter and Hemley [10] were the first to describe this polymorph as a hexagonal arrangement of triazine (C_3N_3) rings (Fig. 1 *a*). Three rings are connected *via* an additional nitrogen atom. In this structure, carbon is present exclusively in the sp²-hybridized state, while nitrogen has both sp²- and sp³-hybridization within and between the rings, respectively.

Some theoretical and experimental studies suggest distinguishing three types of g-polymorph: g-h-triazine, g-h-heptazine (hexagonal structure), and g-o-triazine (orthorhombic structure) (Fig. 2).[4,12,22] The three varieties differ in the way of ring coupling: in g-h-triazine, the triazine rings are connected *via* nitrogen atoms to form a hexagonal lattice (Fig. 2 *a*); g-h-heptazine contains larger heptazine units (C_6N_7) (Fig. 2 *b*); and g-o-triazine has an orthorhombic chain packing (Fig. 2 *c*). The unit cell parameters for the three types of g-C_3N_3 differ:

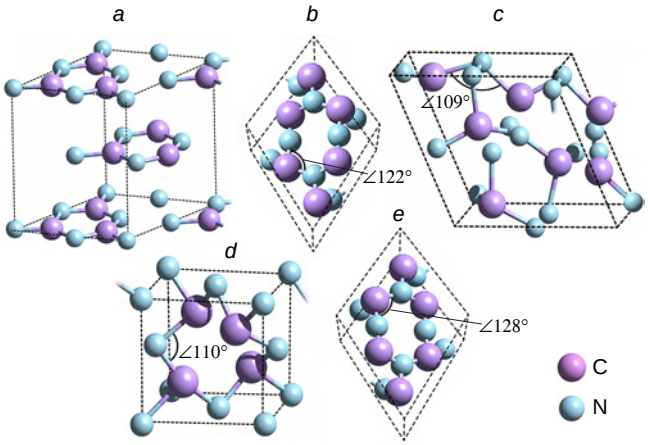


Figure 1. Crystal unit cell of various carbon nitride polymorphs: g-C_3N_4 (*a*), β-C_3N_4 (*b*), c-C_3N_4 (*c*), p-C_3N_4 (*d*), and α-C_3N_4 (*e*).

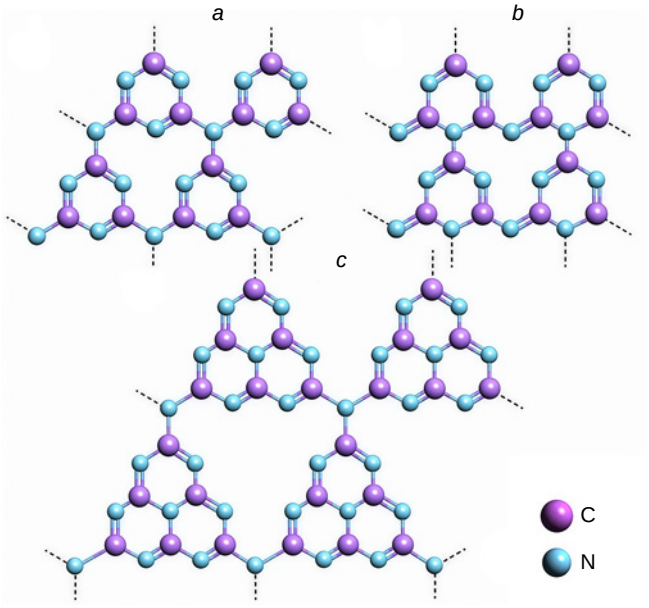


Figure 2. Structures of the three types of graphitic carbon nitride: g-h-triazine (*a*), g-o-triazine (*b*), g-h-heptazine (*c*).[4]

g-h-triazine	g-h-heptazine	g-o-triazine
a = 4.746 Å	a = 7.083 Å	a = 4.147 Å
c = 6.586 Å	b = 12.269 Å	b = 4.754 Å
	c = 6.871 Å	c = 6.474 Å

It should be emphasized that the actual structure of g-C_3N_4 always differs from the idealized model. Low-temperature polycondensation is always accompanied by the formation of defects, such as nitrogen vacancies, incomplete condensation of amino groups, and protonated surface amino groups (NH/NH_2). These defects play a dual role. On the one hand, they generate additional active sites for adsorption of molecules and for capture of photoinduced charge carriers (electrons, holes), thus increasing the photocatalytic activity. On the other hand, they act as nonradiative recombination centres, thus reducing the quantum yield. Controlling the defect density by varying the nature of the precursor, temperature, and synthesis time is key to tuning functional properties of g-C_3N_4.

While analyzing the literature on g-C_3N_4, it is necessary to distinguish between several terms that are often not distinguished by the authors. ***The idealized crystal model of g-C_3N_4*** is a strictly periodic structure with a hexagonal packing of triazine or heptazine rings fully fused without surface groups or defects. This structure is used in most theoretical calculations of the band structure and mechanical properties of the material. ***Polymeric carbon nitride*** is a broad term that covers polycondensation products with varying degrees of order that contain defects, surface amino groups, and partially unreacted fragments of starting precursors. The partially ordered condensation products are materials obtained at temperatures below the optimal ones (*e.g.*, 400–500°C), where polymerization does not occur completely, resulting in a high defect density and low degree of crystallinity. In this review, unless otherwise specified, the term g-C_3N_4 refers to actual products of thermal polycondensation.

When discussing theoretical models or idealized structures, this is explicitly stated.

The β-C_3N_4 polymorph crystallizes in a structure similar to that of β-silicon nitride (β-Si_3N_4), silicon atoms being replaced by carbon atoms. According to theoretical calculations, this phase is thermodynamically unstable.[10,11,13] The structure is a lattice of CN_4 tetrahedra connected to one another *via* three-coordinate nitrogen atoms (Fig. 1 *b*). Each sp^3-hybridized carbon atom is linked to four nitrogen atoms in a distorted tetrahedral geometry, while each sp^2-hybridized nitrogen atom is connected to three carbon atoms in a trigonal planar configuration. The unit cell parameters are $a = 6.406$ Å and $c = 2.406$ Å [space group P3(143)].[10,17]

The cubic polymorph has a defective zinc blende structure, which differs from the ideal cubic structure of diamond due to rhombohedral distortion.[10,11,13] Like in β-C_3N_4, in this structure, each carbon atom is tetrahedrally coordinated to four nitrogen atoms, while each nitrogen atom is trigonally coordinated to three carbon atoms (Fig. 1 *c*). However, the C–N–C bond angle approaches 109°, which is characteristic of sp^3-hybridization, rather than 120° typical of sp^2-hybridization. This structure belongs to the P43m space group and has two free parameters: the cubic lattice constant ($a = 5.395–5.444$ Å) and the internal variable ($x = 0.25–0.35$),[23] which quantitatively determine the radial relaxation around the vacancy.

The structure of the pseudocubic phase (p-C_3N_4) belongs to the space group R3m (Fig. 1 *d*). Within the unit cell, one carbon atom and one nitrogen atom are three-coordinate, while the other three nitrogen atoms are only two-coordinate due to the absence of a carbon atom. The structure is defined by five internal coordinates, the lattice parameter ($a = 3.41–3.44$ Å), and a rhombohedral angle of 110°.

According to theoretical calculations, α-C_3N_4 is the most energetically stable polymorph among all carbon nitride structures.[11,13] The structure is a mirror image of β-C_3N_4 (Fig. 1 *e*). The unit cell contains 28 atoms and has P31c symmetry with lattice parameters $a = 6.465$ Å and $c = 4.709$ Å.[10]

Thus, there are five stable forms of carbon nitride with markedly different structures, which, as we show below determine the key properties of the material.

2.2. Identification

In all experimental studies, the obtained product was identified by comparing powder X-ray diffraction data with those reported by Matsumoto *et al*.,[24] who calculated the peak positions in the X-ray diffraction patterns for ideal structures of the five main C_3N_4 polymorphs (Fig. 3). The calculated data for β-C_3N_4 showed that the number of intense peaks in $2\theta = 10–50°$ range is smaller (Fig. 3 *a*) than that for the α-polymorph (Fig. 3 *b*).[24] According to the calculations by Matsumoto *et al*.,[24] the main difference between cubic carbon nitride and the other forms was the absence of X-ray diffraction peaks at $2\theta < 40°$ (Fig. 3 *c*). p-C_3N_4 was characterized by the presence of peaks in the range of 20–90° (Fig. 3 *d*). The DFT calculation for g-C_3N_4 results in a set of reflections in the $2\theta = 10–40°$ range (Fig. 3 *e*).[24] In experimental studies, the authors observed only two intense peaks at 13.6° (100) and 27.4° (002).[3,4,21] The (002) plane has the interplanar spacing $d = 3.24$ Å, which is typical of packing of aromatic structures in graphite. It is noteworthy that powder X-ray diffraction virtually does not allow for identification of g-h-heptazine, g-h-triazine, or g-o-triazine C_3N_4 types. As it was noted in two publications,[25,26] the peak at 17.4° (or ~18°) in the

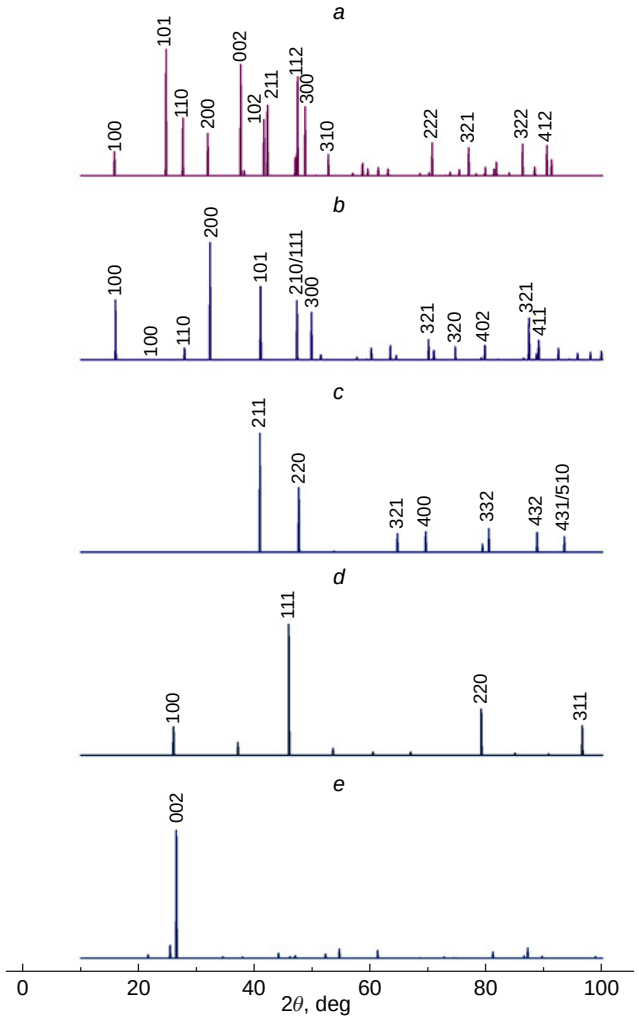


Figure 3. X-ray diffraction patterns of the polymorphs β-C_3N_4 (*a*), α-C_3N_4 (*b*), c-C_3N_4 (*c*), p-C_3N_4 (*d*), and g-C_3N_4 (*e*).[24]

X-ray diffraction pattern corresponds to the presence of a triazine phase without indicating the type of packing (hexagonal or orthorhombic).

Apart from powder X-ray diffraction, in a number of studies, the authors identified the products of synthesis by comparing the interplanar spacings derived from transmission electron microscopy or selected area electron diffraction[16,18,19,27–30] with the interplanar spacings reported by Matsumoto *et al*.[24]

Some authors identified the products of synthesis using Raman or IR spectroscopy.[19,27,31–34] Characteristic peaks (Table 2) were found for each polymorph, which can serve to identify the material. The samples containing mixtures of α- and β-polymorphs exhibited strong Raman bands at 946 and 984 cm^{-1}, indicating the presence of both phases.[30]

It should be pointed out that in a number of studies[17,27,29] where the authors claimed to obtain polymorph mixtures (α+β or β+p, or the like), identification was based only on reflections detected in the X-ray diffraction patterns and their correlation with published data.[24] No quantitative assessment of the percentage ratio of obtained phases was performed due to the lack of a well-established and validated procedure for determining the ratio of polymorphs in mixtures from X-ray peak intensity ratios,[35] similar to that used for titanium dioxide.

Table 2. Characteristic Raman and IR peaks (cm^{-1}).[19,30,31,34]

α-C_3N_4 (Raman)[a]/IR[b]	β-C_3N_4 (Raman)[a]/IR[b]	c-C_3N_4 (IR)[b]	p-C_3N_4 (IR)[b]	g-C_3N_4 (IR)[a]
	251			
	305			
436/449				479
–/511	–/573	~550		543
671/609, 619	623			
689				705
–/739				751
827/852, 887	–/852			
982	943			
–/1012	–/1008			
			1110	
–/1201	1265	~1200		1234
	–/1380			
1423/1464	–/1421	~1400		1481
				1555
				1616

[a] Results of calculations; [b] experiment.

3. Properties of polymorphs

3.1. Physical characteristics

According to theoretical calculations, dense carbon nitride polymorphs should have high hardness.[10] However, the experimental data on their mechanical properties are still fragmentary. Li *et al*.[36] established that the Vickers hardness of amorphous carbon nitride films with a thickness of 4–5 mm is 45–50 GPa, whereas hardness of ~230 nm-thick β-C_3N_4 films reaches 60 GPa.[37] This is much lower than the values for diamond (Vickers hardness in the range of 90–100 GPa). The modulus of elasticity of a 400 nm-thick β-C_3N_4 film was experimentally found to be 349 GPa,[38] which was not equal to the calculated values (see Table 1).

Ming *et al*.[39] determined experimentally the density of p-C_3N_4, which amounted to 2.62 g cm^{-3}; this proved to be lower than the theoretically calculated value (3.81 g cm^3).

Another characteristic of a material is its specific surface area (*S*),[†] which is important for applications such as catalysis, adsorption, pharmaceutics. The values vary from 5 to 150 m^2 g^{-1} depending on the method of synthesis and the starting reactants (as shown below) and are not determined by the type of polymorph:[40–53]

α-C_3N_4	β-C_3N_4	g-C_3N_4
135.6	5.0	5.0–153.2

3.2. Optical properties

The band gap energy of dense C_3N_4 polymorphs is a key issue for determining the scope of applicability of the materials. However, there are considerable discrepancies between the calculated values (for ideal crystals) and the experimentally obtained ones (Table 3).

The theoretical studies of electronic structure and properties are usually conducted using DFT in various approximations.[22,54,57–62] The most commonly used approximations are GW, local density approximation (LDA), and generalized gradient approximation (GGA). The GW approximation calculates the intrinsic energy of the system using the single-particle Green's function (G) and the screened Coulomb interaction (W), which allows a more accurate determination of the band gap energy (E_g). LDA is based on the exchange-correlation interaction in solid state theory considering the electron density at a particular point in space. GGA improves LDA results by including electron density gradient for better approximation of the exchange-correlation energy. Most often, band gap at Γ-point (the gamma point) means the energy difference between the top of the valence band and the bottom of the conduction band at the centre of the Brillouin zone. The band gap may be direct if the valence band maximum and the conduction band minimum are at the same point, or indirect if they are at different points in the Brillouin zone.[63]

Table 3. Band gaps for dense polymorphs of C_3N_4 determined using various approximations.

C_3N_4 polymorph	E_g, eV					Refs
	Indirect transition		Direct transition		Experiment[a]	
	GW	LDA	GW	LDA		
β		3.25				10, 54
	4.85	3.12				22
					2.77	55
					3.9	56
					3.43/3.81	41
		3.21		3.59		57
	6.4	3.11	6.75			58
		3.20				59
		3.43	4.58	3.56		60
α		3.85				10
	5.49	3.76				22
					2.76	17, 40
		3.67				54
		3.80		4.40		57
Cubic		2.90				10
	4.30	2.87				22
		2.82/2.91		5.03		57
Pseudo-cubic			4.13	2.53		22
				2.43		54
				2.59		57
			4.19	2.53		61
			~4			62

[a] Optical transition by the Tauc plot method.

The results of the first-principles pseudopotential calculation of the total energy reported by Liu and Cohen[59] indicate that the β-phase has an indirect band gap. Using the GW approximation, Corkill and Cohen[58] identified both indirect (Γ→L) and direct band gaps at point Γ in β-C_3N_4. According to calculations performed by Molina and Sansores,[57] the α-, β-, and cubic carbon nitride phases have indirect band gaps, while the pseudocubic polymorph features a direct band gap.

Analysis of publications devoted to calculation of the structures of solid carbon nitride phases shows that different approximations can yield different values for the band gap energy of the same phase, ranging from 2.87 to 6.4 eV. A more detailed investigation of the calculated E_g values reveals that

[†] The specific surface areas given in the review were determined using the Brunauer–Emmet–Teller method (S_{BET}, m^2 g^{-1}).

GW approximation tends to provide higher values than LDA. Some authors attributed this discrepancy to the characteristics inherent in the approximations.[22] Comparison of the results within the same approximation may also show some differences that could arise due to variations in the initial calculation parameters, such as the number of k-points and the cut-off energy.[61] Without experimental data on the electronic properties of materials, it is difficult to determine which approximation is more accurate.

The experimental estimation of the band gap (optical band gap) is performed using the Tauc method. Figure 4 shows examples of absorption spectra and corresponding Tauc plots for three β-C_3N_4 samples.[64] It can be seen that doping with copper or formation of composites with titanium dioxide cause the absorption edge to shift to longer wavelengths. The Tauc approach, which is based on analysis of the absorption spectra or diffuse reflectance spectra, is widely used due to its simplicity and accessibility. The major benefit of the Tauc approach is that it allows one to estimate the optical band gap without complex mathematical modelling, making it convenient for fast characterization of new photocatalytic materials, especially in the early stages of their development. Furthermore, this method is well suited for evaluating a series of samples synthesized under comparable conditions in order to identify relative trends in the variation of E_g depending on the morphology, defect density, or degree of crystallinity.

According to the data presented by Zhang *et al*,[65] metal and non-metal doping of g-C_3N_4 may considerably decrease the optical band gap (determined experimentally), but the mechanisms of the decrease are different. In the case of non-metals, narrowing of the optical band gap can be explained as follows: the synthesis may be accompanied by the formation of defects, which enhance optical absorption,[66] and, in addition, doping elements can lead to electronic integration.[67,68] In the case of metals, additional energy levels may arise within the band gap.[69] In the development of composites with noble metals (Ir,[70] Pt,[71] Pd,[72] Ir, Pt[73]), structures containing metal quantum dots (spherical in shape and 2.5–3.1 nm in diameter) are formed during the synthesis, which leads to a Schottky contact with a wider optical band gap (2.71–2.88 eV).[70–73]

However, it is important to take into account the considerable limitations and potential sources of error associated with this method. First, the accuracy of determining the optical band gap crucially depends on the correct choice of coefficient reflecting the nature of electron transitions (direct or indirect; allowed or forbidden). For example, as follows from theoretical calculations, in the case of carbon nitride, various polymorphs can experience both direct and indirect transitions, and an incorrect choice of exponent (for example, using 1/2 instead of 2) can lead to a systematic error. For example, Vignesh *et al*.[74] calculated the electronic structure of g-C_3N_4 under the assumption that this is a direct-band-gap semiconductor, whereas composites based on this material are indirect-band-gap semiconductors. Moreover, a key subjective stage is extrapolation of the linear portion of the Tauc plot onto the abscissa axis. The presence of impurity phases, defects, or considerable scattering on the particle surface can distort the spectral edge shape, thus making the selection of a linear segment ambiguous. This results in variable E_g values reported in the literature for the same material (as shown in Table 3). In the case of β-C_3N_4, the optical band gaps found in several studies[41,55,56] are in good agreement with the range of calculated values, whereas for the α-polymorph, the optical band gap energies are markedly lower than the calculated values. It is of interest that identical experimental values (E_g = 2.76 eV) were found for both a single-phase sample[37] and an α+β mixture.[59] Similar results were obtained for the well-known photocatalyst, titanium dioxide.[75–80] It has been established, that in mixed-phase TiO_2 samples, the optical band gap can vary from 2.7 eV to 3.3 eV depending on the type of impurity phase (anatase, brookite, rutile) and the ratio of these phases. Furthermore, the Tauc method does not include the contribution of excitons and other many-body effects, which is particularly important for semiconductors with strong electron- hole interaction. Hence, the values obtained in this way should be regarded as effective or apparent values, requiring careful interpretation and, whenever possible, verification using additional techniques such as ultraviolet photoelectron

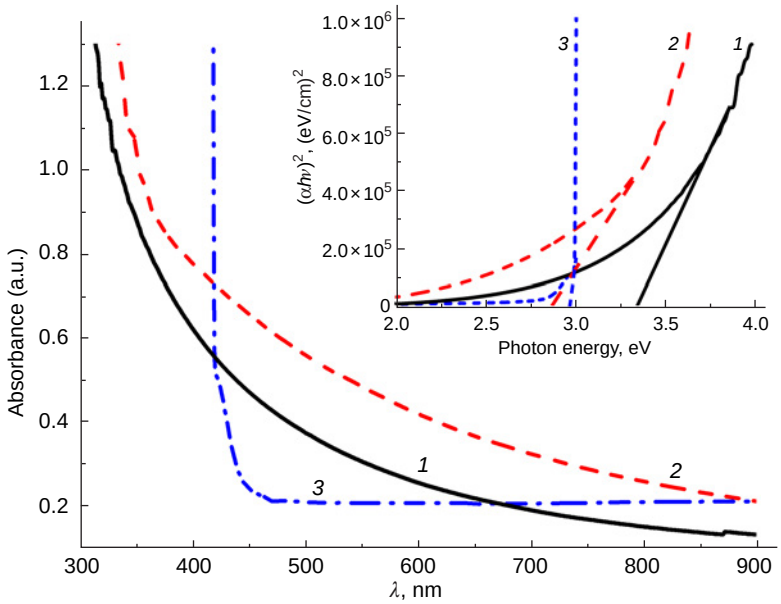


Figure 4. Absorption spectra of aqueous suspensions and Tauc plots for β-C_3N_4 (*1*), TiO_2/β-C_3N_4 (*2*), Cu-doped β-C_3N_4 (*3*) (the plots were created by the authors using published data[64]). (Copyright Russian Chemical Reviews: *Russ. Chem. Rev*., 2026, **95** (10), RCR5243).

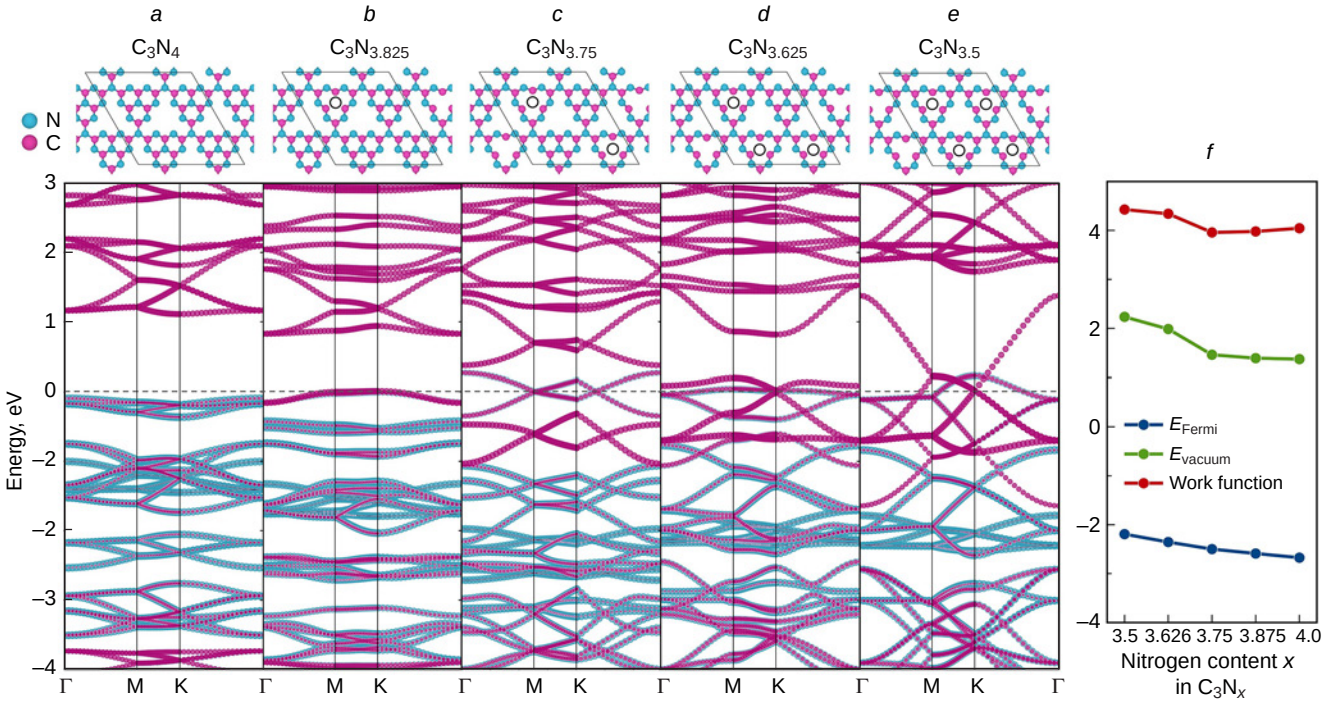


Figure 5. Changes in the band structure of g-C_3N_4 with various defect densities: (*a*) C_3N_4 (Copyright Springer, 2025),[88] (*b*) $C_3N_{3.825}$, (*c*) $C_3N_{3.75}$, (*d*) $C_3N_{3.625}$, (*e*) $C_3N_{3.5}$. Nitrogen atoms are shown in light blue, carbon atoms are shown in pink, and nitrogen vacancies are empty circles. (*f*) Dependences of the Fermi level energy, vacuum level, and work function on the nitrogen concentration in g-C_3N_4 samples (Figures *b*–*f* were created by the authors using published data[88]).

spectroscopy or first-principles calculations using corrections. For example, a comparison of the band gaps calculated for ideal structures with experimentally determined values sometimes reveals considerable differences (as illustrated by g-C_3N_4):[81–83]

E_g (calc.), eV	2.36	2.34
E_g (exp.), eV	2.59	2.7

Meanwhile, the authors assert that the obtained values are in very good agreement with one another, even though this difference could be attributed to the different compositions of the material (g-C_3N_4 as a polycondensation product with unreacted precursor impurity).

Meanwhile, computational models usually consider idealized structures, whereas experimentally obtained samples contain numerous defects. These defects influence the electron density and, hence, the band structure of the material.[84–86] As established experimentally,[87] even minor changes in the C/N ratio (from 0.721 to 0.742), caused by temperature rise, result in a decrease in the band gap energy from 2.8 to 2.75 eV. Computed data on the band structure for various concentrations of nitrogen vacancies indicated a dispersion of electronic energy levels depending on the wave vector for C_3N_4, $C_3N_{3.825}$, $C_3N_{3.75}$, $C_3N_{3.625}$, and $C_3N_{3.5}$ (Fig. 5).[88] As the defect density increases on going from C_3N_4 to $C_3N_{3.825}$, the band gap energy decreases from 1.21 to 0.82 eV. It was also found that carbon contribution to the valence band increases in $C_3N_{3.825}$ compared to C_3N_4. An increase in defect density endows the material with metallic conduction: in particular, no band gap is present in $C_3N_{3.75}$. Further increase in the defect density gives rise to a material significantly different from initial g-C_3N_4, with unpredictable changes to the band structure.

However, using experimentally measured band gap energies as references, it is possible to select and calibrate computational methods that would improve the accuracy of future predictions. For example, if the electronic band structure of a pure material is known, the effects of doping or the formation of heterojunctions between different layered materials can be accurately predicted using computational methods.[10,89]

Thus, the band gap energy depends on a large number of factors related to both experimental conditions and calculation methods. To reliably determine the band gap of C_3N_4 and other polymorphs, it is necessary to combine experimental methods (first of all, the Tauc method, bearing in mind its limitations) and computational approaches, with the latter being calibrated using experimental data for ideal structures and then extrapolated to more complex systems with defects and heterojunctions. Consequently, determining the band structure of C_3N_4, like that of many other two-dimensional materials prone to defect formation and deformation, is an extremely challenging task. Perhaps, the active use of machine learning and artificial intelligence methods and data obtained from DFT calculations would make it possible to study systems containing a large number of atoms and consider numerous factors. This would improve the accuracy of determination of the band structure of real C_3N_4-based materials that contain defects and impurities.

4. Preparation methods

The evolution of the methods of synthesis of carbon nitride is depicted in Fig. 6. In the initial stages, high pressure/high temperature (HPHT) methods were used, by analogy with the synthesis of diamond, in order to prove the possibility of formation of C_3N_4 (Table 4). The obtained samples contained considerable amounts of impurities, including diamond, silicon, and various forms of silicon nitride, mainly due to the use of silicon substrates.[24] Thermolysis/pyrolysis and hydrothermal/solvothermal and shock-wave methods are more advanced

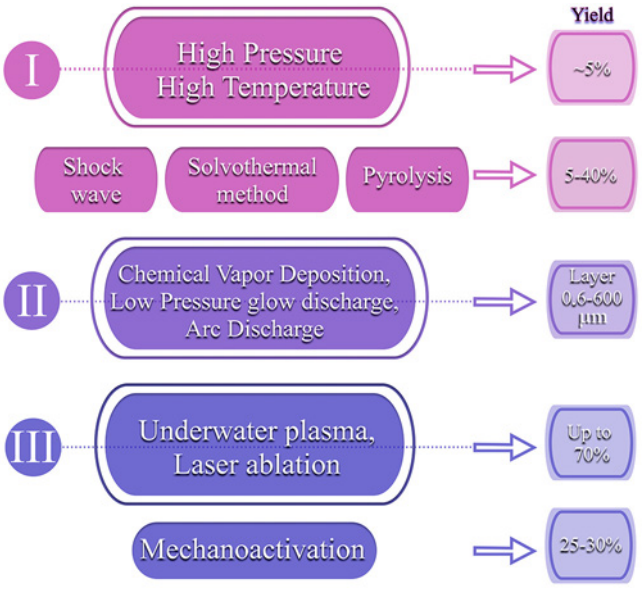


Figure 6. The evolution of the synthesis methods of carbon nitride.

versions of HPHT. It is noteworthy that thermolysis/pyrolysis is used most often to produce the g-C_3N_4 polymorph (Table 5), owing to the simplicity of this procedure. In most studies, the authors reported only qualitative characteristics of the final product, demonstrating that the method they used was applicable for the synthesis of this polymorph, but did not provide a quantitative estimate of the product yield. According to the few available data, thermolysis/pyrolysis gives the product in a yield of 3–12%. An exception is provided by the results reported by Elamin *et al.*,[95,96] who obtained the product in a yield of more than 60%. However, this high yield may be a result of imprecise product identification.

The solvo-/hydrothermal methods were tested for the synthesis of various polymorphs (Table 6). By varying the experimental conditions such as the solvent or the duration of the synthesis, it is possible to obtain materials with an extensive surface area.

The transition to the use of low-pressure plasma (thermal or low-temperature), including the chemical vapour deposition (CVD) technique, has demonstrated the possibility of producing thin films and coatings from gaseous reactants (Table 7). In this case, a more complex design of the production unit is required, because it must include vacuum or low-pressure generation equipment.

The next stage in the development of this method involved the use of underwater plasma initiated by electrical discharge or laser radiation (Table 8). This type of plasma does not require generation of a low pressure, and the product is detected by the appearance of a liquid-phase dispersion. According to published results, the product yield can reach 70% in this case.

The first studies dealing with a different method, laser ablation, used organic liquids (cyclohexane, decalin) as precursors.[111] This choice was based on stereochemical criteria: the molecules of these compounds had the same building blocks as the carbon allotropes. Subsequently organic liquids were abandoned, because it was impossible to obtain carbon nitride polymorphs that were free of diamond polytypes. Special mention should be made of mechanochemical activation. In some cases, researchers combine this method with exposure to high pressures or high temperatures. According to published data,[27,29,112] there is no correlation between the time of mechanoactivation and the yield of the final product, all other factors being equal (Table 9).

Systematic consideration of the literature on the synthesis of carbon nitride (Tables 4–9) reveals several fundamental contradictions that were not taken into account previously, because researchers were focused on the photocatalytic properties of graphitic polymorph. First, attention is attracted by the discordance between the ease of obtaining g-C_3N_4 and the exceptional complexity of the synthesis of dense polymorphs (α, β, c, p). Whereas thermal pyrolysis of urea or melamine at 550°C and at atmospheric pressure is a routine procedure, the synthesis of even a mixture of α and β phases requires either extremely high pressures or fairly complex equipment. This engineering disparity has led to the fact that the vast majority of publications are devoted to g-C_3N_4, while the unique mechanical and electronic properties of the dense phases largely exist as theoretical predictions.

The second issue is the low reliability of identification of the target polymorphs. The most vivid example is provided by studies on the pyrolysis of guanidine hydrochloride,[96,97] which claim the preparation of β-C_3N_4 in >60% yield. However, critical analysis of the presented X-ray diffraction patterns and IR spectra clearly indicates that the product is a conventional graphitic carbon nitride. This indicates that, in some cases, researchers identify the prepared samples relying on single, non-specific features, while ignoring the full set of reflections or

Table 4. Key characteristics of the synthesis of dense carbon nitride polymorphs using various HPHT techniques.

Method	Precursors	Conditions (*P*, GPa/ *T*, °C/additional parameters)	C_3N_4 polymorph	Yield, mg	Notes	Refs
Shock wave	$NaN(CN)_2$+CI_4+NaN_3+Cu (cat.)	20–25/–/–	β	50–100	—	90
HPHT	g-C_3N_4	20–38/1873/– 20–38/>3273/–	c	no data	P > 30 GPa and T > 3273°C; the product contained no g-phase or diamond impurity	33, 39
Shock wave	g-C_3N_4	22.4/–/–	Triclinic phase[a]	no data	Lattice parameters:[b] *a* = 4.81 Å, *b* = 3.53 Å, *c* = 2.85 Å	91
Shock wave	Dicyandiamide+Ni (cat.)	15.5/1973/–	α	no data	—	92
High-pressure laser irradiation	Cyanic acid	–/1473–1973/[c]	Orthorhombic phase[a]	no data	Lattice parameters:[b] *a* = 7.635 Å, *b* = 4.487 Å, *c* = 4.040 Å	93

Note. The time was not specified in any of the experiments. [a] New polymorphs were found, the structure of which needs to be confirmed by sets of methods. [b] Crystal lattice parameters of the new phase. [c] Precursor pretreatment with a YAG laser.

Table 5. Key characteristics of the synthesis of C_3N_4 polymorphs by thermolysis/pyrolysis

Precursors	*T*, °C	*P*, Pa/ conditions	Time	Product (polymorph)	Yield (%)	Notes and properties (S_{BET}, м^2 г$^{-1}$)	Refs
Tetracyanoethylene/1,3,5-triazine	1400	5×10^9	30 min	g-C_3N_4	No data		12
Melamine	550	1×10^5	4 h	g-C_3N_4	No data	S_{BET} = 12.7	42
	550	1×10^5	3 h	g-C_3N_4	No data	S_{BET} = 13.7	43
	550	1×10^5	4 h+3 h (annealing)	g-C_3N_4	No data	S_{BET} = 19	51
	650	1×10^5	3 h	g-C_3N_4	11	S_{BET} = 19	94
Urea	550	1×10^5	3 h	g-C_3N_4	No data	S_{BET} = 110.2	43
Urea	550	1×10^5	4 h+3 h (annealing)	g-C_3N_4	No data	S_{BET} = 69.4	51
Thiourea	550	1×10^5	4 h	g-C_3N_4	No data	S_{BET} = 20.6	42
	550	1×10^5	4 h+3 h (annealing)	g-C_3N_4	No data	S_{BET} = 28.1	51
Dicyanamide	550	1×10^5	4 h+3 h (annealing)	g-C_3N_4	No data	S_{BET} = 19.29	51
	550	1×10^5	4 h	g-C_3N_4	No data	S_{BET} = 6.75	27
Dicyandiamide	550	1×10^5	4 h	g-C_3N_4	10	S_{BET} = 70.2	52
	550	1×10^5	3 ч	g-C_3N_4	No data	S_{BET} = 9.5	43
Cyanamide	550	1×10^5	4 h	g-C_3N_4	No data	S_{BET} = 16.1	42
Guanidine chloride	550	1×10^5	4 h	g-C_3N_4	No data	S_{BET} = 14.8	42
	650	1×10^5	3 h	g-C_3N_4	3.25	S_{BET} = 65.1	94
	550	1×10^5	3 h	β-C_3N_4	63.5	According to the physicochemical analysis, the pyrolysis product is g-C_3N_4	95
			2 h		61		96
Urea : melamine (3 : 1)	550	1×10^5	2 h	g-C_3N_4	12	S_{BET} = 57.0	97
Ethylenediamine	500	–/Nitrogen	2 h	β	No data	Morphology: flexible tubes	55
2-Amino-1,3,5-triazine + urea + $(NH_4)_2CO_3$ + cat. (Fe, Co, Ni, Pd)	1400	7×10^9	10 min	α/β mixture	No data	Morphology: rods	17
Triazine [a]	400 → 800	–/Nitrogen (flow)	60 min	β-C_3N_4	No data	Morphology: a mixture of sheets and nanotubes	98
Polyvinyl chloride + NH_4Cl + Fe_2O_3 (cat.)	650	Autoclave [b]	6 h	α/β mixture	No data	Morphology: nanowires	99
Urea + $CuCl_2$ (cat.)	500 → 550 [c]	Air (atmospheric pressure)	2 h → 1 h [c]	β-C_3N_4/CuO composite	No data		100

[a] A two-chamber setup was used for the synthesis: pyrolysis unit consisting of two chambers connected in series at different temperatures; the precursor (triazine) was loaded into the first chamber (evaporator, 400°C), where it evaporated upon heating but did not decompose; in the second chamber (reactor, 800°C), pyrolysis took place and the product was deposited on the chamber walls. [b] The pressure at which the synthesis was carried out was not specified in the publication. [c] The notation 500 → 550 and 2 h → 1 h means two successive stages of heat treatment: one at 500°C for 2 h and the other at 550°C for 1 h.

characteristic vibrational modes. In this case, the presence of a peak at $2\theta = 27°$ was mistakenly interpreted as being due to the β-phase, whereas this polymorph is characterized by a complex multiplet of peaks in the 23–48° range rather than two diffuse peaks.

The problem of phase purity is significant for most methods used to prepare dense polymorphs. As can be seen from many studies, single-phase samples of α-, β-, and c-C_3N_4 are unique cases. Even the use of complex approaches, such as chemical vapour deposition, often results in the formation of a mixture of phases (α+β) and inevitable contamination by the substrate material (Si_3N_4) or inorganic carbon (diamond, graphite). In fact, only laser ablation in liquid and low-temperature plasma in liquid have demonstrated the ability to produce single-phase products (*e.g.*, the β-phase),[71] but these methods are still far from scaling-up. This provides the conclusion that in most experimental studies, especially earlier ones, the authors were dealing not with pure polymorphs but with defective nanocrystalline mixtures and, therefore, the direct comparison of the physicochemical properties reported by different research groups is inappropriate.

Finally, the evolution of synthesis methods, as illustrated in the Tables, is essentially a spiral motion. Researchers have moved away from energy-intensive and hazardous high-pressure and high-temperature methods toward soft chemistry. However, having been faced with the problem of low crystallinity and impurities in solvothermal methods, they made the next logical step, that is, switched again to physical treatment (laser, plasma), but this time in a liquid-phase medium. The paradox is that the thermal pyrolysis methods, which are most promising in terms of cost-effectiveness and scalability, are suitable only for producing the g-modification. They are either inapplicable to dense phases or give a mixture of products, which attests that the processes are kinetically rather than thermodynamically controlled. Thus, the main challenge in this field of materials science is not the search for new exotic phases, but the

Table 6. Key characteristics of the synthesis of C_3N_4 polymorphs by hydro-/solvothermal methods.

Precursors	Solvent	*T*,°C	*P*, MPa/ conditions	Time	Product (polymorph)	Yield (%)	S_{BET}, $m^2\ g^{-1}$	Refs
Cyanuric chloride + sodium amide	Benzene	195	–	15 h	g-C_3N_4	No data	No data	19
Cyanuric chloride + sodium hydrazine	Benzene CCl_4 Cyclohexane CH_3CN	195	Autoclave[a]	15 h	g-C_3N_4 with Na^+ impurity	0.48 7.4 1.3 39.1	No data	45
Cyanuric chloride + melamine	Acetonitrile	180	Autoclave[a]	96 h	g-C_3N_4	Up to 39.1	No data	45
Melamine	Water	180	Autoclave[a]	15 h	g-C_3N_4	5	6.78	50
Urea : melamine	Water	180	Autoclave[a]	16 h	g-C_3N_4	No data	29.03 – 126.98	101
Urea : cyanuric acid (3 : 1)	Water	180	Autoclave[a]	18 – 24 h	g-C_3N_4	No data	23.8 – 153.17	97
2,4,6-Trichloro-1,3,5-triazine + Li_3N	Benzene	355	5 – 6	12 h	α + β mixture	No data	No data	102, 103
Ethylenediamine + CCl_4 (reflux), then annealing at 600°C	–	90 (reflux) → 600 (annealing)	0.1	6 h → 5 h[b]	α-C_3N_4	17 – 20	No data	28
Cyanuric chloride + NaN_3	Acetonitrile	150 – 180	Autoclave[a]	15 h	β + p mixture	No data	No data	104
Cyanuric chloride + NaN_3	Acetonitrile	220	Autoclave[a]	15 h	Multiphase β-C_3N_4	No data	No data	104
1,3,5-trichlotriazine + NaN_3 + Zn (cat.)	Benzene	220	40 MPa	6 h	p + β	No data	No data	105

[a] The pressure at which the synthesis was carried out was not specified in the publication. [b] The notation 90 → 600 and 6 h → 5 h means two successive stages: refluxing at 90°C for 6 h, then annealing at 600°C for 5 h.

Table 7. Key characteristics of the synthesis of C_3N_4 polymorphs by CVD and low-pressure plasma treatment.

Method	Gas mixture = precursors	Substrate (electrodes)	*P*, kPa	*T*,°C/Power	Time	Product (polymorph)	Notes and properties	Refs
Dual ion beam	Ar + (C sputtering) N_2^+ (bombardment)	Si, Be, Cu	0.01 – 0.001	~400/no data	No data	C_3N_4 films (amorphous/ nanocryst.)[a]	Thickness: ~50 nm	14
Microwave plasma CVD	$CH_4 + N_2$	Si, Pt	3	~900/2450 MHz	1.5 h	α + β	Thickness 400 nm	20
Microwave plasma CVD	$CH_4 + N_2$ (excess N_2)	Si	2.5	800 – 950/ 500 – 700 W	1.5 h	α/β mixture (contaminated with Si_3N_4)	Thickness: 650 nm	31, 37
Microwave plasma CVD	$CH_4 + N_2 + H_2$	Polycryst. Ni	4 – 13.3	no data	No data	Phase mixture (α, β, p, g)		106
Plasma-enhanced CVD (PECVD)	C_2H_4 (0.6 L min^{-1}) + N_2 (4 L min^{-1})	Si (with Si_3N_4 buffer)	0.4	420/no data	No data	c-C_3N_4 (film)	Transparent in the near-IR range	107
Low-pressure glow discharge	$N_2 + C_2H_2$	steel (cathode), graphite (anode)	0.5	500/800	No data	α-C_3N_4 with impurities (at 500°C)/ orthorhombic phase (at 800°C)	Orthorhombic phase (a = 2.74 Å, b = 7.18 Å, c = 9.7 Å)	108
Plasma sputtering (glow discharge)	$CH_4 + N_2 + H_2$	Si (with Ni coating)	0.82	750	45 min	g-C_3N_4 (films)	Contains impurities	47

[a] For the dual ion-beam method, no phase identification of the product was performed: at ~400°C, the synthesis gave amorphous or nanocrystalline C_3N_4 films without sufficient long-range order to be classified as a specific polymorph.

development of reliable methods for the synthesis of previously predicted polymorphs with controlled defect structure in amounts sufficient for practical testing.

5. Morphology of polymorph particles

Along with the electronic structure, morphology is one of the main factors influencing the properties of materials. The particle morphology of dense polymorphs significantly depends on the synthesis method and the presence of additional phases (Fig. 7).[16,32,40,41,56,98,104,113,114] Treatment with low-pressure glow discharge plasma resulted in the formation of polyhedral α-C_3N_4 structures (Fig. 7 *a*).[40] The effect of the synthesis method on the particle morphology can be clearly seen in relation to the β-polymorph (Fig. 7 *b*,*e*–*i*). The chemical vapour deposition yields hexagonal rods (Fig. 7 *b*,*e*).[113] In this case, the composition

Table 8. Key characteristics of the synthesis of C_3N_4 polymorphs by methods using liquid-phase plasma at atmospheric pressure upon laser irradiation (1) or an electrical discharge in underwater plasma (2).

Method	Precursors/target/ medium	Laser type and characteristics (λ, nm/power, mJ pulse^{-1}/ frequency, Hz/pulse width, ns/ radiation density, J cm^{-2})/discharge	Time	Product (Polymorph)	Yield (%)	Notes and properties	Refs
1	Graphite target in a 35% NH_3 solution	Nd : YAG, 532/10/100/–	1 – 7 h	β	No data	Morphology: leaf-like. As time passes, the size of the leaves increases.	56
1	Graphite target in a 35% NH_3 solution	Nd : YAG, 532/–/–/120	2 h	α	No data	Morphology: spheroids	109
1	Graphite target in liquid NH_3	Nd : YAG, 532/–/–/120	5 h	α	No data	Morphology: nanorods	100
1	Graphite target in liquid NH_3	Nd : YAG, 1064/–/–/80	5 h	α/β mixture	No data		109
1	Graphite powder in 25% NH_3	Nd : YAG, 532/5/–/10^{10} W cm^{-2}	30 min	c	No data	Morphology: prisms	110
2	Aqueous solution of urea	Electrical discharge, U = 1.3 kV, I = 0.25 A	10 min	β	70	S_{BET} = 5.0 m^2 g^{-1}	41
2	Acetonitrile	Electrical discharge, U = 1.3 kV, I = 0.25 A	10 min	β	62	Morphology: 2D plates and prisms	41
1	Hexamine in liquid NH_3 on a W substrate (at T = –60°C), dry N_2 atmosphere	Excimer, 248/ 5/2/35	No data	α/β mixture	No data		15

Table 9. Key characteristics of the synthesis of C_3N_4 polymorphs by mechanochemical activation, electrolysis, arc discharge, and solution combustion.

Method	Precursors/Conditions	Time	Product (Polymorph)	Yield (%)	Notes and properties	Refs
Mechanochemical activation	Graphite → grinding to the nanoscale (20 – 110 h) → activation in NH_3 or liquid N_2 (300 kPa) → annealing at 450°C in N_2	48 h 70 h 5 h	α/β mixture	10 47 25	Morphology: flakes and spheres	27, 29, 112
Electrochemical method	Urea in methanol + CH_3COOH (for the avalanche effect), U = 800 V, I = 200 mA, Si substrate (cathode)	3 – 8 h	c (films, dendrites)	No data	Film thickness: 620 nm in 3 h	32
Thermal plasma (arc discharge)	Carbon powder containing trace amounts of nitrogen in Ar – H_2, 2 MHz, 400 W	No data	c	No data		18
Vacuum arc discharge	Graphite electrodes in N_2 (P = 24 kPa, U = 25 V, I = 150 A) → annealing at 700°C	2 h (annealing)	p + β	No data	Identification by the IR spectrum (1110 cm^{-1} peak)	19
Solution combustion	Saturated solution of urea → heating to 400°C → holding at 450°C	1 – 3 h	α	No data	Nanoporous material (average pore diameter of ~2 nm)	40

is determined by the synthesis conditions (pressure, substrate temperature). An irregular morphology is formed in the solvothermal synthesis (Fig. 7 *d*,*f*).[104] The in-liquid plasma treatment furnishes 2D plates and prisms under the action of an electric discharge[41] (Fig. 7 *g*) or leaf-like particles on the surface of a substrate under laser irradiation (Fig. 7 *h*).[56] It was noted, however, that in the case of laser irradiation, increase in experiment duration (from 1 to 7 hours) leads to a decrease in the number of leaf-like particles accompanied by an increase in leaf size. Upon pyrolysis, dense polymorphs are formed as elongated structures shaped like either flexible nanotubes[98] (Fig. 7 *i*) or nanowires.[99] Dendritic structures of the cubic phase are formed upon the electrochemical synthesis on a silicon substrate (Fig. 7 *c*).[32]

For the layered g-phase the particle morphology is also determined by the synthesis method. For example, cone-shaped structures are formed on a substrate surface in the synthesis using low-pressure glow discharge (Fig. 8 *a*).[47] However, this is more an exception than a rule. Since g-C_3N_4 is prepared, most often, using thermal polycondensation or solvo-/hydrothermal method (see Section 3, Table 5), it is possible to trace the effect of the precursor nature on the resulting particle morphology. For example, when urea and thiourea are used, the thermal polycondensation gives coarse-aggregate spherical particles (Fig. 8 *b*),[51,114] while using a mixture of urea and glycine results in the formation of layered structures (Fig. 8 *c*). This means that in high-temperature synthesis, glycine acts not only as a source of carbon and nitrogen, but also as an exfoliating agent. If urea, melamine, and dicyanamide are used separately, nanosheets are formed only in the case of urea; in all other cases, dense aggregated structures are formed.[22] The addition of ammonium chloride during pyrolysis of dicyandiamide makes it possible to

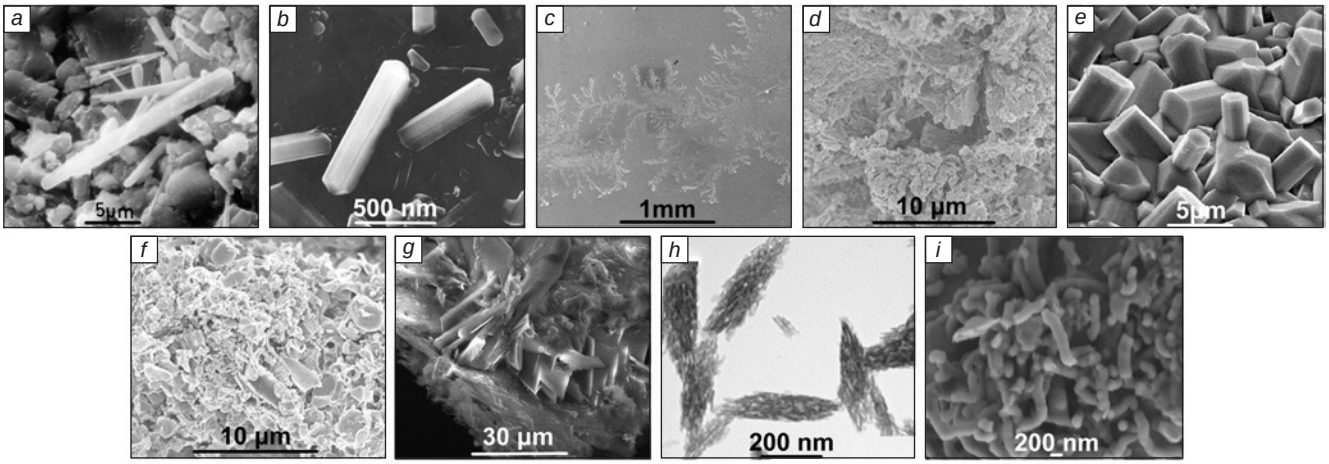


Figure 7. SEM images of dense C_3N_4 polymorphs: α-C_3N_4 (*a*) (Copyright Elsevier, 2002),[40] β/α-C_3N_4 (*b*) (Copyright Taylor & Francis, 1997),[16] cubic polymorph (*c*) (Copyright Springer Nature, 2009),[32] p-/β- (*d*) (Copyright IOP Publishing, 2016),[114] hexagonal β-C_3N_4 (*e*) (Copyright Elsevier, 2010),[113] β-C_3N_4 (*f*) (Copyright IOP Publishing, 2016).[104] SEM images of β-C_3N_4 prepared by the in-liquid plasma technique (*g*) (from the authors' archive for Ref. 41), laser ablation in liquid (*h*) (Copyright IOP Publishing, 2006),[56] and pyrolysis (*i*) (Copyright Elsevier, 2021).[98]

produce nanosheets from bulk material (Fig. 8*d*). Therefore, this reagent can be classified as exfoliating agent.[115]

The hydrothermal synthesis using melamine results in the formation of disordered layered structures (Fig. 8*e*).[116] It was shown that both one-portion and gradual addition of cyanuric acid to melamine induces sequential transformation of the irregular structures into hexagonal rods (Fig. 8*f*), hollow nanotubes (Fig. 8*g*), and spherical structures (Fig. 8*h*) as the acid concentration increases.

The diversity in the morphology of carbon nitride particles, regardless of their polymorphic form, is due to differences in the mechanisms of crystal nucleation and growth, which are determined by the synthesis conditions (Tables 4–9). In the case of gas-phase methods, key factors include the degree of supersaturation of the reaction medium, the substrate temperature, and the energy of the ions bombarding the growing surface. This promotes the formation of equilibrium polyhedral or rod-like structures. In liquid-phase and solvothermal processes, the morphology is determined by the nucleation rate, diffusion limitations, and the presence of surfactants, which can selectively inhibit the growth of certain faces, resulting in the formation of dendritic or sheet structures. In the case of thermal polycondensation of g-C_3N_4, the morphology is additionally controlled by the kinetics of the polycondensation of the precursors and release of gaseous products, which promote exfoliation of the material. Thus, the same polymorph may have substantially different morphology, since the external synthesis conditions dictate a non-equilibrium crystallization pathway determining the final shape of the particles.

6. Potential applications of carbon nitride

6.1. Wear-resistant coatings

Initially, study of the properties and development of synthesis of dense carbon nitride polymorphs was driven by unique mechanical and thermophysical characteristics predicted for these materials. As follows from Table 1, the calculated bulk moduli of the α-, β-, cubic, and pseudocubic polymorphs are

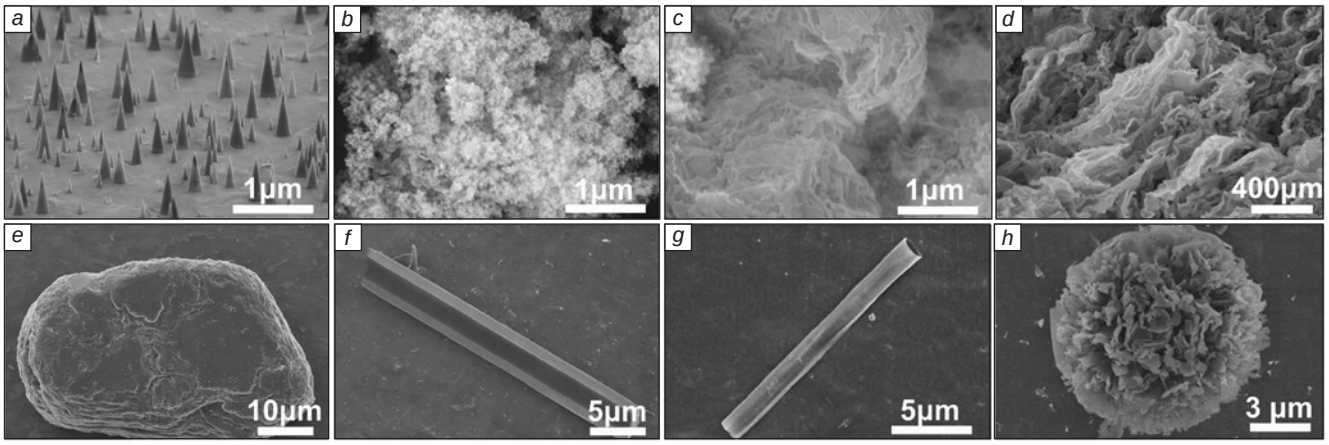


Figure 8. SEM images of g-C_3N_4 of various morphology produced by plasma-chemical process (*a*) (Copyright ACS Publications, 2015);[47] pyrolysis of urea (*b*) (Copyright Elsevier, 2020),[114] urea + glycine (*c*) (Copyright Elsevier, 2020),[114] and dicyanamide + NH_4Cl (*d*) (Copyright The Royal Society of Chemistry, 2014);[115] hydrothermal method using melamine (*e*) (Copyright Elsevier, 2024),[116] melamine and cyanuric acid in 5 : 1 ratio (*f*) (Copyright Elsevier, 2024),[116] melamine and cyanuric acid in 3 : 1 ratio (*g*) (Copyright Elsevier, 2024),[116] and melamine and cyanuric acid in 2 : 1 ratio (*h*) (Copyright Elsevier, 2024).[116]

comparable to or even exceed those for diamond and cubic boron nitride. This opens up the potential for using these materials as superhard coatings for cutting tools, protective coatings, optical components, and high-temperature electronic devices. In an early study, Zhang *et al*.[31] showed that 0.6-μm carbon nitride films (α- and β-polymorph mixture) have bulk modulus of 349 GPa. It was shown[107] that thin (600 nm) c-C_3N_4 films are transparent in the near-IR spectral range; hence, this material could potentially be used for the manufacture of infrared windows.

However, as shown above, the practical implementation of this potential faces considerable obstacles. The key problem is still the difficulty of obtaining single-phase crystalline samples in significant amounts. In addition, for thin-film coatings, a considerable problem is the high level of internal stress, which arises upon deposition and induces film cracking and peeling off from the substrate. Thus, despite the impressive theoretical predictions, transition from laboratory samples to industrial applications of dense C_3N_4 phases as superhard materials requires further efforts to develop scalable synthesis methods providing controlled defect density and to create effective buffer layers to reduce stress.

6.2. Photocatalysts

6.2.1. Removal of dyes

According to the latest published reviews on g-C_3N_4 and its composites, the scope of applications for these photocatalysts is expanding every year to cover photocatalysis, electrochemical devices, and biomedicine. The real products of synthesis of graphitic carbon nitride (by thermal polycondensation) possess an sp^2-hybridized graphite-like lattice, which provides electrical conductivity and visible light absorption, while structural defects and surface amino groups form active sites for catalysis. Therefore, this material is often considered for the use in photocatalytic decomposition of water and organic pollutants, such as dyes, pharmaceuticals, *etc*., in an aqueous medium.[117–119] g-C_3N_4 is among the first and most extensively studied metal-free photocatalysts for the production of hydrogen from water under visible light, although its efficiency is limited by rapid charge carrier recombination,[120] CO_2 reduction, hydrogen peroxide (H_2O_2) synthesis, and for selective oxidation reactions.[121,122] In this Section, we limit ourselves to the results of most recent studies (published since 2024) on graphitic carbon nitride and dense polymorphs and their composites that have been considered as photocatalysts for the removal of dyes.

Despite the relatively narrow band gap (1.9–2.8 eV), there are only few studies on the use of single-phase graphitic carbon nitride as a photocatalyst, and published data are often contradictory, as reflected in Table 10.

In the case of photocatalytic degradation of dyes, it should be noted that, according to the data given in Table 10, the efficiency of dye removal depends not only on the carbon nitride polymorph used, but also on the nature of the dye, the weight of the photocatalyst, the power of the light source, and other factors.

Table 10. Photocatalytic efficiency of various carbon nitride polymorphs.

Catalyst C_3N_4 (m_{cat}, mg)	Experimental conditions: dye(s) (dye/mixture concentration, mol L^{-1})// radiation source: lamp (power, W), exposure time (min)	Sorption (%) /k_{ef} (min^{-1})/ Efficiency (%)	Refs
α (20)	RB (2.5×10^{-5})//Xe lamp (300), 70	–/–/100	40
β-/CuO (5)	MB (3.1×10^{-5})//halogen lamp (300), 240	15/0.002/43.3	100
β+p (250)	MO (7.6×10^{-4})//Xe lamp (200), 3000	–/0.001/91	104
β (30)	RB (2.5×10^{-6})//Xe lamp (35), 120	10/0.002/23	123
$SrTiO_3$/β (30)	RB (2.5×10^{-6})//Xe lamp (35), 120	15/0.002/33	123
β (30)	RB+RR6C+MB (2.5×10^{-6} each)[a]//Xe lamp (35), 90	RR6C 18/0.003/53 RB 15/0.004/57 MB 20/0.005/38	41
Cu/β (30)	RB+RR6C+MB (2.5×10^{-6} each)[a]//Xe lamp (35), 90	RR6C 8/0.002/30 RB 10/0.001/29.4 MB 16/0.002/31.2	64
Ti/ β (30)	RB+RR6C+MB (2.5×10^{-6} each)[a]//Xe lamp (35), 90	RR6C 9/0.009/55 RB 8/0.01/67 MB 15/0.011/67	64
g (50)	MB (2×10^{-4})//LED lamp (λ = 400 nm), 180	–/0.027/32	52
g (50)	MO (3×10^{-5})//direct sunlight, 150	20/0.015/44	124
g (50)	MB (3.1×10^{-5})//direct sunlight, 150	17/0.012/36	
g (10)	RB (1×10^{-5})//LED lamp, 100	–/0.045/50	125
g (200)	RB (2.1×10^{-5})//Xe lamp (λ > 400 nm), 120	4/0.006/~61	126
g (no data)	RB (2.1×10^{-5})//Xe lamp (500 W, λ = 400 nm), 180	–/0.021/88	127
g (no data)	MO (3×10^{-8})//Xe lamp (500 W, λ = 400 nm), 180	–/0.013/40	127
g (35)	MO (5×10^{-5})//LED lamp (30mW cm^{-2}, λ = 365, 450, and 540 nm), 120	8/–/40	128
g (35)	RB (5×10^{-5})//LED lamp (30 mW cm^{-2}, λ = 365, 450, and 540 nm), 120	22/–/50	128
g (35)	MB (5×10^{-5})//LED lamp (30 mW cm^{-2}, λ = 365, 450, and 540 nm), 120	88/–/100	128
g (30)	RB+RR6C+MB (2.5×10^{-6} each)[a]//Xe lamp (35), 90	RR6C 10/0.003/50 RB 16/0.007/74 MB 18/0.026/69	88

Note. k_{ef} is the effective reaction rate constant. Efficiency (%) means the percentage of dye removal relative to the remaining dye concentration. RB is rhodamine B, MB is methylene blue, MO is methylene orange, RR6C is reactive red 6C. [a] In the studies on photocatalytic decomposition of dye mixtures, the changes in the concentration of each dye were determined by monitoring the intensity variation at the absorption maxima.

The authors noted that for a dye mixture being treated in solution, the photocatalyst can act as sorbent for one dye (most often methylene blue), thus hindering effective removal of other dyes.[41,127,128]

Comparison of the results obtained by different research teams (see Table 10) shows a considerable scatter in the photocatalytic efficiency values, even for identical or similar carbon nitride polymorphs. This is attributable to several factors such as different procedures used for carbon nitride synthesis, resulting in varying defect densities and degrees of condensation; the lack of standard conditions for photocatalytic experiments (light source power, wavelength, catalyst weight, dye concentration); and different nature of the dyes, which are differently adsorbed on the catalyst surface. In some studies, the adsorption stage is not taken into account,[40,52,104,125,127] which also complicates comparison of the data. Comparison of the results obtained for mixtures of dyes in which competitive adsorption may occur requires particular caution.

To summarize the above, the following can be stated: the results of studies on the applicability of dense carbon nitride polymorphs as photocatalysts are illustrative in nature, being often limited to statement of the fact of removal (or bleaching). However, neither the removal kinetics and the factors affecting it, nor the processes of dye adsorption on the material surface, nor the regeneration/stability of the photocatalyst are studied in detail. The question of the total solution salinity after the photocatalytic process also remains open. These data are available for graphitic C_3N_4. Presumably, the next stage in the study of dense carbon nitride polymorphs would involve detailed investigation of the above factors that determine the use of C_3N_4 as a photocatalyst.

6.2.2. Water splitting

Due to the high level of the conduction band, carbon nitride is a very good material for photocatalytic reduction reactions, such as H_2 evolution from water and CO_2 reduction, which was recently discussed in several reviews.[120–122] For dense polymorphs, studies addressing this issue are fragmentary. For example, Wu *et al.*[40] showed that the α-polymorph has a higher photocatalytic activity than g-C_3N_4 toward water splitting and hydrogen evolution on exposure to visible light (Fig. 9 *a*). Single-phase β-C_3N_4 showed a low photocatalytic activity in the water splitting, with the oxygen evolution rate being only 67 μmol g^{-1} h^{-1} and measurable hydrogen evolution rate being absent[55] (Fig. 9 *b*); however, TiO_2/β-C_3N_4 composites performed well in this process: a hydrogen evolution rate was more than 10^3 μmol g^{-1} h^{-1} and the oxygen evolution rate increased more than six-fold.

The operating principle of photocatalysts is often interpreted by analogy with other semiconductor photocatalysts, such as TiO_2.[129,130] On exposure to light, the catalyst surface absorbs photon energy equal to or greater than the band gap energy (Fig. 10). This absorption excites an electron from the valence band to the conduction band, giving rise to a photogenerated hole in the valence band and a photoexcited electron in the conduction band. The photogenerated holes and photoexcited electrons migrate towards the catalyst surface where they react with water molecules. These reactions result in the formation of reactive hydroxyl radicals and superoxide ions ($O_2^{-\bullet}$). Then these radicals react with dissolved substances, leading to the decomposition of organic pollutants. In the case of water splitting, the photogenerated holes react with water molecules adsorbed on the photocatalyst surface to oxidize the oxygen ion

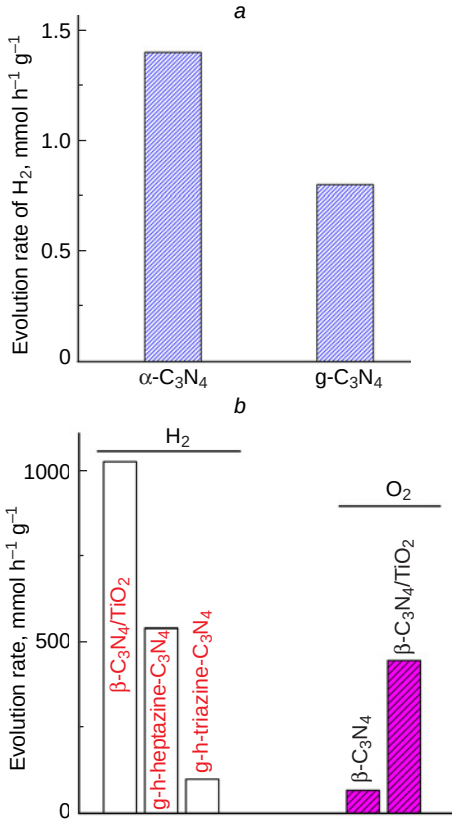


Figure 9. Rates of product evolution during photocatalytic water splitting: (*a*) hydrogen in the presence of α- and g-C_3N_4 and (*b*) hydrogen and oxygen in the presence of g-C_3N_4 and β- C_3N_4-based composite (the Figure was created by the authors using published data[40,55]).

to O_2. The proton thus formed is reduced in a reaction with electrons to give H_2.[131] The reduction of CO_2 to CO involves photogenerated electrons.[121] In carbon nitride-based composite, heterojunctions are formed; this generates favourable conditions for the separation of photoinduced charges (electrons and holes) and suppresses their recombination, which substantially increases the photocatalytic activity.

Apart from the band structure of carbon nitride, surface states, particularly the presence of active sites, must also be taken into account for considering photocatalytic processes. In this context, it is necessary to mention not only the presence or concentration of Lewis and Brønsted acid and base sites, but also the nature of these sites. As noted by Li *et al.*,[132] various active sites on the carbon nitride surface substantially affect the photocatalytic activity. For example, edges and nitrogen defects, as well as hydrophilic groups considerably increase the photocatalytic activity for hydrogen generation upon water splitting or dye photodegradation.[125] It is believed that the role of active sites in photocatalytic processes can be enhanced through modifications such as the creation of heterojunctions, the introduction of new functional groups, and the development of additional absorption sites. It is noteworthy that particle morphology plays an important role in photocatalytic processes. Nanostructures with angular morphologies (*e.g.*, rods, prisms) exhibit enhanced photocatalytic activity due to shorter charge transport paths along their edges.[40] The influence of morphology on the photocatalytic activity of dense polymorphs is difficult to assess because of the limited number of published results. These regularities for g-C_3N_4 have been addressed in recent reviews.[133–136]

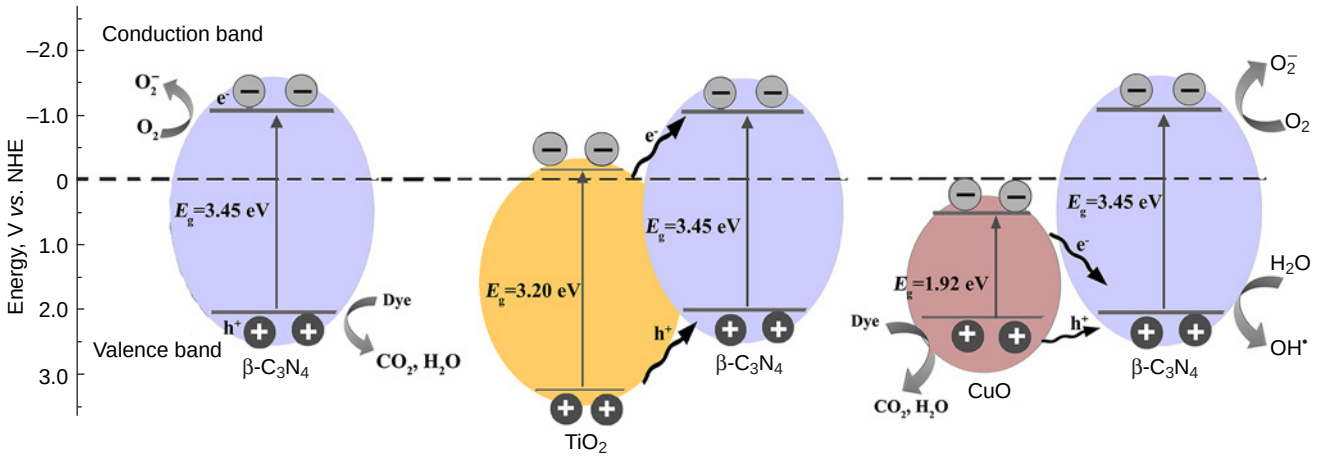


Figure 10. Band structure of β-C_3N_4 and composites based on it.

If the principles underlying heterogeneous photocatalytic processes for C_3N_4 are similar to those for other semiconductor materials, why are researchers increasingly focusing on g-C_3N_4? This polymorph can be easily synthesized from nontoxic precursors; furthermore, advances in understanding the structure of carbon nitride have made it possible to synthesize it under milder conditions compared to earlier methods, which required high pressures of 20–38 GPa and temperatures of 1873–3273°C. This also rules out the need for expensive specialized equipment. g-C_3N_4 has a moderate band gap energy and is thermally stable; its band structure is in line with the redox potentials of water, in particular with the energy levels of the valence and conduction bands relative to the standard electrode potential[55,100] (see Fig. 10). Among the drawbacks mentioned above, one may note low specific surface area, which leads to high charge recombination rates. However, by varying the synthesis method and the starting reactants, it is possible to obtain catalysts with a highly extensive surface (see Table 5), thus reducing recombination rates. All forms of C_3N_4 are insoluble in both organic and inorganic solvents, which attests to their chemical inertness. This feature is a benefit, as photocatalysis can be conducted in both aqueous and non-aqueous media, facilitating easy removal of the catalyst without the concern that any part of the material has dissolved. In addition, the hydrophobicity of the carbon nitride surface can be increased by surface modification.[137–139]

A limitation of using carbon nitride as a photocatalyst is the position of the absorption edge, typically around 420 nm. However, this edge may shift to longer wavelengths up to 450–620 nm depending on the degree of condensation and the density of defects.[40,55] Slow crystallization kinetics can increase synthesis time, which potentially allows for the control of the efficiency of the obtained catalyst. Methods such as solution combustion, laser ablation in liquids, and liquid-phase plasma are promising alternatives to the hydro-/solvothermal method.[41,56,109] Analysis of published results shows that photocatalytic efficiency also depends on the class and structural features of the dye. The development of composite materials using inorganic oxides, organic compounds, or natural polymers is a key strategy for improving performance, as reflected in recent papers and reviews.[119,64,140,141]

Thus, analysis of the published data indicates that the photocatalytic activity of single-phase C_3N_4 polymorphs markedly depends on their crystal structure. α-Polymorph has a high activity toward water splitting, whereas β-polymorph has low efficiency in a pure state, but serves as a promising base for composites. As regards photodegradation of organic dyes, g-C_3N_4 has been most studied; however, its performance varies greatly depending on the experimental conditions and the nature of the contaminant. The key limitations hindering the widespread use of single-phase forms include the high rate of charge recombination and insufficient visible light activity due to the absorption edge position at ~420 nm. Promising strategies to overcome these issues include control of the morphology (the production of nanorods or nanoprisms) and the creation of heterojunctions. These are further goals of research in this field.

6.3. Optoelectronics and sensor technology

Wide band gap materials could be used in fields such as photovoltaics and optoelectronics. It was shown in a number of studies[142–144] that β-C_3N_4 quantum dots (3 to 6 nm in size) exhibit effective fluorescence in green and blue regions of the spectrum (the quantum yield reaches 73%). Hence, this material can be considered as a promising medium for lasers. Moreover, it was established[144] that fluorescence is highly sensitive to the presence of some ions (Ag^+, Cu^{2+}), which expands the potential of sensing applications of this material.

7. Conclusion

The analysis of published data reveals that carbon nitrides, which exist in several polymorphs, including both idealized crystal structures and real products with varying degrees of order, represent a unique class of materials. These materials combine structural diversity with a wide range of functional properties; each polymorph has a specific electronic structure, morphology, and, consequently, photocatalytic activity. Graphitic g-C_3N_4 is one of the most studied materials; it is easily synthesized from inexpensive precursors and has high chemical stability. However, its practical application is limited by fast charge recombination and moderate specific surface area, and an intrinsic absorption edge located near 420 nm. In contrast, dense polymorphs have high mechanical properties, according to theoretical predictions, and may be promising for developing superhard coatings and semiconductor devices. However, their synthesis remains energy-intensive and often leads to the formation of mixed phases or defective nanocrystalline products.

A key contradiction in this field is the pronounced discrepancy between the theoretically and experimentally determined band

gaps: the density functional theory using standard approximations systematically underestimates E_g, whereas experimental data show higher values for the same phases. This discrepancy is due to the limitations of computational models, which assume ideal structures and do not take into account the actual defects in the synthesized samples such as nitrogen vacancies, impurities, and crystal lattice imperfections.

Another important conclusion is that the morphology of particles is not specific to any polymorph. α- and β-phases can appear as rods, prisms, or dendrites depending on the synthesis method, with the specific surface area varying over a wide range. This means that external crystallization conditions play a predominant role in determining the morphology, often overriding the structural constraints of the crystal lattice.

In terms of photocatalytic activity, pure C_3N_4 polymorphs are inferior to composites: although the α-polymorph showed certain efficiency in water splitting, the pure β-phase has a low activity; however, its composites with TiO_2 or CuO show a significant increase in the activity. As applied to degradation of organic dyes, g-C_3N_4 has been most studied; however, its performance markedly varies depending on the nature of the dye, the power of the radiation source, and the catalyst weight. In the presence of dye mixtures, competitive adsorption is possible, which distorts the results.

Thus, the main challenges include the development of scalable and cost-effective methods for the synthesis of dense polymorphs with controlled defect density. One also needs to combine experimental and computational approaches in order to reliably determine the band structure. Additionally, one needs to move on from investigating pure phases to forming heterostructures. Combining various forms of carbon nitride, rather than searching for an ideal, pure polymorph, is the most realistic approach for designing new-generation photocatalysts with high efficiency, visible light activity, and long-term stability.

8. List of abbreviations and symbols

E_g — band gap,
f — laser frequency,
Γ (gamma) — centre of the Brillouin zone,
K — corner (vertex) of a hexagonal Brillouin zone,
L — centre of a hexagonal face of a Brillouin zone,
M — centre of an edge of a hexagonal Brillouin zone,
P — Pressure (Pa),
S_{BET} — Brunauer–Emmett–Teller specific surface area ($m^2\ g^{-1}$),
T — temperature (°C),
DFT — density functional theory,
GGA — generalized gradient approximation (used to calculate exchange-correlation energy in atoms, molecules, and solids),
GW — a method for calculation of intrinsic energy of the system based on the use of the single-particle Green's function (G) and the screened Coulomb interaction (W),
HSE — Heyd–Scuseria–Ernzerhof hybrid density functional theory,
LDA — local density approximation (a calculation method based on exchange-correlation interactions in solid-state theory),
Nd:YAG — neodymium aluminium yttrium garnet (pulsed laser type),
PBE — Perdew–Burke–Ernzerhof parameterization,
YAG — aluminium yttrium garnet (pulsed laser type).

9. References

1. A.Fujishima, K.Honda. *Nature*, **238**, 37 (1972); https://doi.org/10.1038/238037a0
2. W.J.Ong, L.L.Tan, Y.H.Ng, S.T.Yong, S.P.Chai. *Chem. Rev.*, **116**, 7159 (2016); https://doi.org/10.1021/acs.chemrev.6b00075
3. S.Cao, J.Low, J.Yu, M.Jaroniec. *Adv. Mater.*, **27**, 2150 (2015); https://doi.org/10.1002/adma.201500033
4. J.Wen, J.Xie, X.Chen, X.Li. *Appl. Surf. Sci.*, **391**, 72 (2017); https://doi.org/10.1016/j.apsusc.2016.07.030
5. J.Fu, J.Yu, C.Jiang, B.Cheng. *Adv. Energy Mater.*, **8**, 1701503 (2018); https://doi.org/10.1002/aenm.201701503
6. Z.Zhao, Y.Sun, F.Dong. *Nanoscale*, **7**, 15 (2015); https://doi.org/10.1039/C4NR03008G
7. C.E.Nebel. In *Nanodiamonds*. Elsevier, 2017, pp. 1–24; https://doi.org/10.1016/B978-0-32-343029-6.00001-5
8. R.T.Paine, C.K.Narula. *Chem. Rev.*, **90**, 73 (1990); https://doi.org/10.1021/cr00099a004
9. S.Adachi. Properties of semiconductor alloys: group-IV, III-V and II-VI semiconductors. John Wiley and Sons, 2009
10. D.M.Teter, R.J.Hemley. *Sci.*, **271**, 53 (1996); https://doi.org/10.1126/science.271.5245.53
11. A.Y.Liu, M.L.Cohen. *Sci.*, **245**, 841 (1989); https://doi.org/10.1126/science.245.4920.841
12. T.H.Y.M.Sekine, H.Kanda, Y.Bando, M.Yokoyama, K.Hojou. *J. Mater. Sci. Lett.*, **9**, 1376 (1990); https://doi.org/10.1007/BF00721588
13. A.Y.Liu, R.M.Wentzcovitch. *Phys. Rev. B*, **50**, 10362 (1994); https://doi.org/10.1103/PhysRevB.50.10362
14. J.P.Riviere, D.Texier, J.Delafond, M.Jaouen, E.L.Mathe, J.Chaumont. *Mater. Lett.*, **22**, 115 (1995); https://doi.org/10.1016/0167-577X(94)00233-9
15. A.K.Sharma, P.Ayyub, M.S.Multani, K.P.Adhi, S.B.Ogale, M.Sunderaraman, D.D.Upadhyay, S.Banerjee. *Appl. Phys. Lett.*, **69**, 3489 (1996); https://doi.org/10.1063/1.117261
16. Y.A.Chen, L.Guo, E.G.Wang. *Philos. Mag. Lett.*, **75**, 155 (1997); https://doi.org/10.1080/095008397179714
17. D.W.He, F.X.Zhang, X.Y.Zhang, Z.C.Qin, M.Zhang, R.P.Liu, Y.F.Xu, W.K.Wang. *J. Mater. Res.*, **13**, 3458 (1998); https://doi.org/10.1557/JMR.1998.0471
18. Y.Peng, T.Ishigaki, S.Horiuchi. *Appl. Phys. Lett.*, **73**, 3671 (1998); https://doi.org/10.1063/1.122858
19. X.Q.Meng, Z.H.Zhang, H.X.Guo, A.G.Li, X.J.Fan. *Solid State Commun.*, **107**, 75 (1998); https://doi.org/10.1016/S0038-1098(98)00152-5
20. Y.S.Gu, Y.P.Zhang, Z.J.Duan, X.R.Chang, Z.Z.Tian, N.X.Chen, C.Dong, D.X.Shi, X.F.Zhang, L.Yuan. *J. Mater. Sci.*, **34**, 3117 (1999); https://doi.org/10.1023/A:1004609218229
21. X.Wang, K.Maeda, A.Thomas, K.Takanabe, G.Xin, G.M.Carlsson, K.Domen, M.Antonietti. *Nat. Mater.*, **8**, 76 (2009); https://doi.org/10.1038/nmat2317
22. Y.Xu, S.P.Gao. *Int. J. Hydrogen Energy*, **37**, 11072 (2012); https://doi.org/10.1016/j.ijhydene.2012.04.138
23. S.Vepřek. *J. Vacuum Sci. Technol. A Vacuum Surf. Films*, **17**, 2401 (1999); https://doi.org/10.1116/1.581977.
24. S.Matsumoto, E.Q.Xie, F.Izumi. *Diam. Relat. Mater.*, **8**, 1175 (1999); https://doi.org/10.1016/S0925-9635(99)00103-X
25. J.Gao, Y.Zhou, Z.Li, S.Yan, N.Wang, Z.Zou. *Nanoscale*, **4**, 3687 (2012); https://doi.org/10.1039/c2nr30777d
26. L.Zhang, Z.Jin, H.Lu, T.Lin, S.Ruan, X.S.Zhao, Y.J.Zeng. *ACS omega*, **3**, 15009 (2018); https://doi.org/10.1021/acsomega.8b01933
27. Y.Fahmy, T.D.Shen, D.A.Tucker, R.L.Spontak, C.C.Koch. *J. Mater. Res.*, **14**, 2488 (1999); https://doi.org/10.1557/JMR.1999.0334
28. Y.Qiu, L.Gao. *Chem. Commun.*, **39**, 2378 (2003); https://doi.org/10.1039/B307086G
29. L.W.Yin, M.S.Li, G.Luo, J.L.Sui, J.M.Wang. *Chem. Phys. Lett.*, **369**, 483 (2003); https://doi.org/10.1016/S0009-2614(02)02044-4
30. Y.Zhang, Y.Gu. *Philos. Mag. Lett.*, **81**, 505 (2001); https://doi.org/10.1080/09500830110051809
31. Y.Zhang, H.Gao, Y.Gu. *J. Phys. D Appl. Phys.*, **34**, 299 (2001); https://doi.org/10.1088/0022-3727/34/3/308

32. Y.Tian, J.Wang, W.Yu, R.Cao, Y.Song, X.Ning. *Sci. China Technol. Sci.*, **52**, 1698 (2009); https://doi.org/10.1007/s11431-009-0109-1
33. P.V.Zinin, L.C.Ming, S.K.Sharma, V.N.Khabashesku, X.Liu, S.Hong, S.Endo, T.Acosta. *Chem. Phys. Lett.*, **472**, 69 (2009); https://doi.org/10.1016/j.cplett.2009.02.068
34. J.Jiang, L.Ou-yang, L.Zhu, A.Zheng, J.Zou, X.Yi, H.Tang. *Carbon*, 80, 213 (2014); https://doi.org/10.1016/j.carbon.2014.08.059
35. D.A.H.Hanaor, C.C.Sorrell. *J. Mater. Sci.*, **46**, 855 (2011); https://doi.org/10.1007/s10853-010-5113-0
36. D.Li, X.W.Lin, S.C.Cheng, V.P.Dravid, Y.W.Chung, M.S.Wong, W.D.Sproul. *Appl. Phys. Lett.*, **68**, 1211 (1996); https://doi.org/10.1063/1.115972
37. W.T.Zheng, W.X.Yu, H.B.Li, Y.M.Wang, P.J.Cao, Z.S.Jin, E.Broitman, J.E.Sundgren. *Diam. Relat. Mater.*, **9**, 1790 (2000); https://doi.org/10.1016/S0925-9635(00)00314-9
38. D.X.Shi, X.F.Zhang, L.Yuan, Y.S.Gu, Y.P.Zhang, Z.J.Duan, X.R.Chang, Z.Z.Tian, N.X.Chen. *Appl. Surf. Sci.*, **148**, 50 (1999); https://doi.org/10.1016/S0169-4332(99)00135-X
39. L.C.Ming, P.Zinin, Y.Meng, X.R.Liu, S.M.Hong, Y.Xie. *J. Appl. Phys.*, **99**, 033520 (2006); https://doi.org/10.1063/1.2168567
40. G.Wu, S.S.Thind, J.Wen, K.Yan, A.Chen. *Appl. Catal. B Environ.*, **142**, 590 2013; https://doi.org/10.1016/j.apcatb.2013.05.070
41. N.Sirotkin, A.Khlyustova, V.Shibaeva, A.Agafonov. *Diam. Relat. Mater.*, **158**, 112644 (2025); https://doi.org/10.1016/j.diamond.2025.112644
42. D.S.Pattanayak, D.Pal, C.Thakur. *Inorg. Chem. Commun.*, **162**, 112201 (2024); https://doi.org/10.1016/j.inoche.2024.112201
43. L.Ma, Z.Li, Z.Jiang, X.Wu, S.Chang, S.A.Carabineiro, K.Lv. *Chin. J. Struct. Chem.*, **43**, 100416 (2024); https://doi.org/10.1016/j.cjsc.2024.100416
44. D.Wang, X.Zhang, H.Zhang, P.Song, P.Yang. *Int. J. Hydrogen Energy*, **68**, 463 (2024); https://doi.org/10.1016/j.ijhydene.2024.04.198
45. Y.Cui, Z.Ding, X.Fu, X.Wang. *Angew. Chem. Int. Ed.*, **51**, 11814 (2012); https://doi.org/10.1002/anie.201206534
46. V.Ragupathi, P.Panigrahi, N.G.Subramaniam. *Optik*, **202**, 163601 (2020); https://doi.org/10.1016/j.ijleo.2019.163601
47. Z.Xu, L.Guan, H.Li, J.Sun, Z.Ying, J.Wu, N.Xu. *J. Phys. Chem. C*, **119**, 29062 (2015); https://doi.org/10.1021/acs.jpcc.5b10952
48. L.Cui, S.Liu, F.Wang, J.Li, Y.Song, Y.Sheng, H.Zou. *J. Alloy Compnd.*, **826**, 154001 (2020); https://doi.org/10.1016/j.jallcom.2020.154001
49. T.Zhao, Q.Zhou, Y.Lv, D.Han, K.Wu, L.Zhao, Y.Shen, S.Liu, Y. Zhang. *Angew. Chem. Int. Ed.*, **59**, 1139 (2020); https://doi.org/10.1002/anie.201911822
50. L.Chen, D.Zhu, J.Li, X.Wang, J.Zhu, P.S.Francis, Y.Zheng. *Appl. Catal. B Environ.*, **273**, 119050 (2020); https://doi.org/10.1016/j.apcatb.2020.119050
51. L.Cao, Y.Li, Z.Zheng. *Russ. J. Phys. Chem. A*, **96**, 1112 (2022); https://doi.org/10.1134/S0036024422050193
52. W.Liu, N.Iwasa, S.Fujita, H.Koizumi, M.Yamaguchi, T.Shimada. *Appl. Surf. Sci.*, **499**, 143901 (2020); https://doi.org/10.1016/j.apsusc.2019.143901
53. Y.H.Gao, W.L.Zhao, Y.Chen. *Diam. Relat. Mater.*, **116**, 108425 (2021); https://doi.org/10.1016/j.diamond.2021.108425
54. F.Ding, Y.P.Feng. *Comput. Mater. Sci.*, **30**, 364 (2004); https://doi.org/10.1016/j.commatsci.2004.02.032
55. R.Jiang, W.Li, K.Zhu, W.Ye, G.Zhu, G.Jia, F.Xu, J.Wang, T.Tao, Y.Wang, X.Kong, X.Wu, S.Du, P.Gao, J.P.Francisco. *J. Alloy. Compnd.*, **920**, 166045 (2022); https://doi.org/10.1016/j.jallcom.2022.166045
56. L.Yang, P.W.May, L.Yin, T.B.Scott, J.A.Smith, K.N.Rosser. *Nanotechnol.*, *17*, 5798 (2006); https://doi.org/10.1088/0957-4484/17/23/015
57. B.Molina, L.E.Sansores. *Mod. Phys. Lett. B*, **13**, 193 (1999); https://doi.org/10.1142/S0217984999000269
58. J.L.Corkill, M.L.Cohen. *Phys. Rev. B*, **48**, 17622 (1993); https://doi.org/10.1103/PhysRevB.48.17622
59. A.Y.Liu, M.L.Cohen. *Phys. Rev. B*, **41**, 10727 (1990); https://doi.org/10.1103/PhysRevB.41.10727
60. H.Yao, W.Y.Ching. *Phys. Rev. B*, **50**, 11231 (1994); https://doi.org/10.1103/PhysRevB.50.11231
61. T.Y.Lü, J.C.Zheng. *Chem. Phys. Lett.*, **501**, 47 (2010); https://doi.org/10.1016/j.cplett.2010.10.055
62. E.Betranhandy, L.Capou, S.F.Matar, C.El-Kfoury. *Solid State Sci.*, **6**, 315 (2004); https://doi.org/10.1016/j.solidstatesciences.2004.01.010
63. K.W. Böer. Handbook of the Physics of Thin-Film Solar Cells, first ed., Berlin, Heidelberg: Springer Berlin Heidelberg, 2013. https://doi.org/10.1007/978-3-642-36748-9_7
64. V.Shibaeva, A.Larionov, N.Sirotkin, D.Yashkova, T.Simonenko, A.Khlyustova, A.Agafonov. *Catalysts*, **16**, 320 (2026); https://doi.org/10.3390/catal16040320
65. W.Zhang, D.Xu, F.Wang, M.Chen. *Nanoscale Adv.*, **3**, 4370 (2021); https://doi.org/10.1039/d1na00264c
66. X.Guo, L.Rao, P.Wang, L.Zhang, Y.Wang. *Int. J. Environ. Res. Publ. Health*, **16**, 581 (2019); https://doi.org/10.3390/ijerph16040581
67. Y.Zhang, T.Mori, J.Ye, M.Antonietti. *J. Am. Chem. Soc.*, **132**, 6294 (2010); https://doi.org/10.1021/ja101749y
68. H.Wang, Y.Bian, J.Hu, L.Dai. *Appl. Catal. B*, **238**, 592 (2018); https://doi.org/10.1016/j.apcatb.2018.07.023
69. R.Ding, S.Cao, H.Chen, F.Jiang, X.Wang. *Colloid Surf. A Physicochem. Eng. Asp.*, **563**, 263 (2019); https://doi.org/10.1016/j.colsurfa.2018.12.020
70. P.Topchiyan, D.Vasilchenko, S.Tkachev, D.Sheven, I.Eltsov, I.Asanov, N.Sidorenko, A.Saraev, E.Gerasimov, A.Kurenkova, E.Kozlova. *ACS Appl. Mater. Interfaces*, **14**, 35600 (2022); https://doi.org/10.1021/acsami.2c07485
71. A.V.Zhurenok, D.B.Vasilchenko, S.N.Berdyugin, E.Y.Gerasimov, A.A.Saraev, S.V.Cherepanova, E.A.Kozlova. *Nanomater.*, **13**, 2176 (2023); https://doi.org/10.3390/nano13152176
72. D.Vasilchenko, A.Zhurenok, A.Saraev, E.Gerasimov, S.Cherepanova, S.Tkachev, P.Plusnin, E.Kozlova. *Chem. Eng. J.*, **445**, 136721 (2022); https://doi.org/10.1016/j.cej.2022.136721
73. N.D.Sidorenko, P.A.Topchiyan, A.A.Saraev, E.Y.Gerasimov, A.V.Zhurenok, D.B.Vasilchenko, E.A.Kozlova. *Catalysts*, **14**, 225 (2024); https://doi.org/10.3390/catal14040225
74. S.Vignesh, S.Chandrasekaran, M.Srinivasan, R.Anbarasan, R.Perumalsamy, E.Arumugam, M.Shkir, H.Algarni, S.AlFaify. *Chemosphere*, **288**, 132611 (2022); https://doi.org/10.1016/j.chemosphere.2021.132611
75. L.Li, C.Y.Liu. *EurJIC*, **2009**, 3727 (2009); https://doi.org/10.1002/ejic.200900369
76. R.G.Nair, S.Paul, S.K.Samdarshi. *Sol. Energy Mater. Sol. Cells*, **95**, 1901 (2011); https://doi.org/10.1016/j.solmat.2011.02.017
77. Y.Liao, W.Que, Q.Jia, Y.He, J.Zhang, P.Zhong, *J. Mater. Chem.*, **22**, 7937 (2012); https://doi.org/10.1039/c2jm16628c
78. B.Choudhury, A.Choudhury. *Phys. E Low-Dimens. Syst. Nanostructures*, **56**, 364 (2014); https://doi.org/10.1016/j.physe.2013.10.014
79. S.Paul, A.Choudhury. *Appl. Nanosci.*, **4**, 839 (2014); https://doi.org/10.1007/s13204-013-0264-3
80. D.R.Eddy, G.A.N.Sheha, M.D.Permana, N.Saito, T.Takei, N.Kumada, Irkham, I. Rahayu, I.Abe, Y.Sekine, T.Oyumi, Y.Izumi. *Chemosphere*, **351**, 141206 (2024); https://doi.org/10.1016/j.chemosphere.2024.141206
81. P.Negro, F.Cesano, S.Casassa, D.Scarano. *Materials*, **16**, 3644 (2023); https://doi.org/10.3390/ma16103644
82. H.Zhang, Z.Yuan, X.Zhao, X.Zhu, H.Wang, Y.Luo, Z.Wang, Z.Jiang. *J. Environ. Sci.*, **163**, 59 (2025); https://doi.org/10.1016/j.jes.2025.08.061
83. P.Niu, L.C.Yin, Y.Q.Yang, G.Liu, H.M.Cheng. *Adv. Mater.*, **26**, 8046 (2014); https://doi.org/10.1002/adma.201404057
84. I.V.Chepkasov, A.G.Kvashnin, A.D.Radina, N.A.Matsokin, F.N.Jalolov, D.G.Kvashnin, A.R.Oganov, Z.Dashevsky. *Appl. Phys. Lett.*, **124**, 022104 (2024); https://doi.org/10.1063/5.0185002
85. M.S.Alkathy, F.L.Zabotto, K.J.Raju, J.A.Eiras. *Mater. Chem. Phys.*, **275**, 125235 (2022); https://doi.org/10.1016/j.matchemphys.2021.125235
86. M.M.Abodouh, G.E.Khedr, N.K.Allam. *Int. J. Hydrog. Energy*, **61**, 922 (2024); https://doi.org/10.1016/j.ijhydene.2024.03.008
87. Y.Zhang, J.Liu, G.Wu, W.Chen. *Nanoscale*, **4**, 5300 (2012); https://doi.org/10.1039/C2NR30948C
88. A.V.Agafonov, N.A.Sirotkin, V.D.Shibaeva, A.D.Radina, A.G.Kvashnin, A.V.Khlyustova. *Russ. J. Inorg. Chem.*, **70**, 2092 (2025); https://doi.org/10.1134/S0036023625604064

89. J.Liu, B.Cheng, J.Yu. *Phys. Chem. Chem. Phys.*, **18**, 31175 (2016); https://doi.org/10.1039/C6CP06147H
90. C.Collins, N.Thadhani, Z.Iqbal. *Carbon*, **39**, 1175 (2001); https://doi.org/10.1016/S0008-6223(00)00234-7
91. X.Gao, H.Yin, P.Chen, J.Liu. *J. Appl. Phys.*, **126**, 155901 (2019); https://doi.org/10.1063/1.5111710
92. H.Yin, P.W.Chen, J.J.Liu, X.Gao, Q.Zhou. *Trans. Beijing Inst. Technol.*, **35**, 991 (2015); https://doi.org/10.15918/j.tbit1001-0645.2015.10.001
93. M.Sougawa, T.Sumiya, K.Takarabe, Y.Mori, T.Okada, H.Gotou, T.Yagi. *J. Phys. Conf. Ser.*, **215**, 012137 (2010); https://doi.org/10.1088/1742-6596/215/1/012137
94. L.Shi, L.Liang, F.Wang, J.Ma, J.Sun. *Catal. Sci. Technol.*, **4**, 3235 (2014); https://doi.org/10.1039/C4CY00411F
95. M.R.Elamin T.G.Ibrahim, M.Salih, N.Y.Elamin, A.Albadri, R.Ramadan, B.Y.Abdulkhair. *J. Mol. Struc.*, **1344**, 143020 (2025); https://doi.org/10.1016/j.molstruc.2025.143020
96. M.R.Elamin, N.Y.Elamin, T.G.Ibrahim, M.Salih, A.Albadri, R.Ramadan, B.Y.Abdulkhair. *Processes*, **13**, 2357 (2025); https://doi.org/10.3390/pr13082357
97. A.V.Zhurenok, A.A.Sushnikova, A.A.Valeeva, A.Y.Kurenkova, D.D.Mishchenko, E.A.Kozlova, A.A.Rempel'. *Kinet. Catal.*, **65**, 112 (2024); https://doi.org/10.1134/S0023158423601225
98. V.Ramasamy, R.Karuppannan. *Diam. Relat. Mater.*, **111**, 108172 (2021); https://doi.org/10.1016/j.diamond.2020.108172
99. J.Wang, L.Zhang, F.Long, W.Wang, Y.Gu, S.Mo, Z.Zou, Z.Fu. *RSC Adv.*, **6**, 23272 (2016); https://doi.org/10.1039/C6RA02475K
100. L.R.Zou, G.F.Huang, D.F.Li, Q.N.Tian, K.Yang, Y.Si, S.Chang, X.A.Zhang, W.Q.Huang. *J. Phys. D Appl. Phys.*, **50**, 355501 (2017); https://doi.org/10.1088/1361-6463/aa7c6f
101. M.Farahmandi, J.B.Ghasemi. *J. Mater. Sci. Mater. Electronic.*, **36**, 573 (2025); https://doi.org/10.1007/s10854-025-14659-5
102. Q.Lv, C.Cao, C.Li, J.Zhang, H.Zhu, X.Kong, X.Duan. *J. Mater. Chem.*, **13**, 1241 (2003); https://doi.org/10.1039/B303210H
103. C.B.Cao, Q.Lv, H.S.Zhu. *Diam. Rel. Mater.*, **12**, 1070 (2003); https://doi.org/10.1016/S0925-9635(02)00309-6
104. C.C.Hu, M.S.Wang, Z.W.Guo. *ECS Trans.*, **72**, 9 (2016); https://doi.org/10.1149/07215.0009ecst
105. X.Lu, L.Gai, D.Cui, Q.Wang, X.Zhao, X.Tao. *Mater. Lett.*, **61**, 4255 (2007); https://doi.org/10.1016/j.matlet.2007.01.076
106. J.Jiang, W.Cheng, Y.Zhang, M.Lan, H.Zhu, D.Shen. *Mater. Lett.*, **61**, 2243 (2007); https://doi.org/10.1016/j.matlet.2006.08.056
107. Z.Zhang, H.Guo, G.Zhong, F.Yu, Q.Xiong, X.Fan. *Thin Solid Films*, **346**, 96 (1999); https://doi.org/10.1016/S0040-6090(98)01457-6
108. Z.Q.Li, J.Y.Zhou, J.Zhang, T.B.Chen, J.Yuan. *J. Alloy Compnd.*, **346**, 230 (2002); https://doi.org/10.1016/S0925-8388(02)00484-X
109. L.Yang, P.W.May, L.Yin, J.A.Smith, K.N.Rosser. *J. Nanoparticle Res.*, **9**, 1181 (2007); https://doi.org/10.1007/s11051-006-9192-4
110. G.W.Yang, J.B.Wang. *Appl. Phys. A*, **71**, 343 (2000); https://doi.org/10.1007/s003390000590
111. A.K.Sharma, R.D.Vispute, D.S.Joag, S.B.Ogale, S.D.Joag, P.Ayyub, M.Multani, G.K.Dey, S.Banerjee. *Mater. Lett.*, **17**, 42 (1993); https://doi.org/10.1016/0167-577X(93)90145-N
112. M.D.Alcalá, J.C.Sánchez-López, C.Real, A.Fernandez, P.Matteazzi. *Diam. Relat. Mater.*, **10**, 1995 (2001); https://doi.org/10.1016/S0925-9635(01)00467-8
113. Y.S.Wu, S.W.Wu. *J. Alloy Compnd.*, **489**, 275 (2010); https://doi.org/10.1016/j.jallcom.2009.09.070
114. M.Yu, S.Chang, L.Ma, X.Wu, J.Yan, Y.Ding, X.Zhang, S.A.C.Carabineiro, K.Lv. *Sep. Purif. Technol.*, **354**, 128695 (2025); https://doi.org/10.1016/j.seppur.2024.128695
115. X.Lu, K.Xu, P.Chen, K.Jia, S.Liu, C.Wu. *J. Mater. Chem. A*, **2**, 18924 (2014); https://doi.org/10.1039/C4TA04487H
116. Z.Dong, T.Yang, S.Xue. *Ceram. Int.*, **50**, 17882 (2024); https://doi.org/10.1016/j.ceramint.2024.02.276
117. B.Huang, K.Xu, Y.Zhao, B.Li, S.Jiang, Y.Liu, S.Huang, Q.Yang, T.Gao, S.Xie, H.Chen, Y.Li. *Molecules*, **30**, 1240 (2025); https://doi.org/10.3390/molecules30061240
118. Y.Zhang, P.Lian, X.Hao, L.Zhang, L.Yang, L.Jiang, K.Zhang, L.Liao, A.Qin. *Inorganics*, **13**, 225 (2025); https://doi.org/10.3390/inorganics13070225
119. Y.Ruan, Y.Hu, H.Cheng. *Catalysts*, **15**, 148 (2025); https://doi.org/10.3390/catal15020148
120. H.Chen, Z.Fan, Z.C.Zhang, J.Guo, C.C.Wang. *Prog. Nat. Sci. Mater. Int.*, **35**, 449 (2025); https://doi.org/10.1016/j.pnsc.2025.03.007
121. R.F.Alekseev, A.A.Saraev, A.Y.Kurenkova, E.A.Kozlova. *Russ. Chem. Rev.*, **93**, RCR5124 (2024); https://doi.org/10.59761/RCR5124
122. Z.Yuan, X.Zhao, X.Zhu, K.Wang, Y.Q.Lan, Z.Jiang. *Chin. Chem. Lett.*, **37**, 112572 (2026); https://doi.org/10.1016/j.cclet.2026.112572
123. K.Ivanov, E.Melnik, N.Sirotkin, A.Khlyustova, A.Agafonov. *Inorg. Chem. Commun.*, **183**, 115823 (2026); https://doi.org/10.1016/j.inoche.2025.115823
124. H.M.Solayman, N.Y.Yahya, K.H.Leong, M.K.Hossain, K.Kang, L.C.Sim, K.D.Zoh, M.B.Khan, A.Abd Aziz. *FlatChem*, **48**, 100762 (2024); https://doi.org/10.1016/j.flatc.2024.100762
125. H.Pang, G.Liu, X.Wang, S.Liu, J.Wang, J.Cui, J.Zhou, Z.Zhou. *Chem.*, **7**, 168 (2025); https://doi.org/10.3390/chemistry7050168
126. C.Y.Tsay, Y.L.Cheng, H.Y.Ou, K.H.Liao. *Phys. B Condens. Matter*, **715**, 417552 (2025); https://doi.org/10.1016/j.physb.2025.417552
127. E.Aksoy, E.Alp. *Glob. Chall.*, **9**, 2500100 (2025); https://doi.org/10.1002/gch2.202500100
128. L.Q.Bu, Q.Y.Li, H.W.Miao, J.C.Yao, J.S.Chen, Q.R.Liu, W.Liu, N.Wang, F.Y.Wu. *Appl. Surf. Sci.*, **713**, 164359 (2025); https://doi.org/10.1016/j.apsusc.2025.164359
129. S.M.George. *Chem. Rev.*, **95**, 475 (1995); https://doi.org/10.1021/cr00035a001
130. H.Wang, X.Li, X.Zhao, C.Li, X.Song, P.Zhang, P.Huo. *Chin. J. Catal.*, **43**, 178 (2022); https://doi.org/10.1016/S1872-2067(21)63910-4
131. E.A.Kozlova, V.N.Parmon. *Russ. Chem. Rev.*, **86**, 870 (2017); https://doi.org/10.1070/RCR4739
132. Y.Li, X.Li, H.Zhang, J.Fan, Q.Xiang. *J. Mater. Sci. Technol.*, **56**, 69 (2020); https://doi.org/10.1016/j.jmst.2020.03.033
133. A.G.Akerdi, M.Mohsenzadeh, K.Mahmoudian, S.H.Bahrami. *Int. J. Environ. Sci. Technol.*, **22**, 7317 (2025); https://doi.org/10.1007/s13762-024-06204-4
134. A.Pundi, C.J.Chang. *Polymers*, **17**, 334 (2025); https://doi.org/10.3390/polym17030334
135. R.Anbarteh, M.Aftabi-Khadar, S.M.Hosseini-Hosseinabad, A.Seza, S.Rahmani Fard, S.Minaeian. *Biomed. Mater.*, **20**, 015036 (2025); https://doi.org/10.1088/1748-605X/ada23a
136. Y.Ma, X.Ji, B.Yang, Y.Jia, J.Nie. *J. Alloy Compnd.*, **1060**, 187255 (2026); https://doi.org/10.1016/j.jallcom.2026.187255
137. X.Bu, J.Li, S.Yang, J.Sun, Y.Deng, Y.Yang, G.Wang, Z.Peng, P.He, X.Wang, G.Ding, J.Yang, X.Xie. *ACS Appl. Mater. Interface*, **8**, 31419 (2016); https://doi.org/10.1021/acsami.6b10516
138. V.Vatanpour, S.Paziresh, A.Dehqan, S.Asadzadeh-Khaneghah, A.Habibi-Yangjeh. *Chemosphere*, **279**, 130616 (2021); https://doi.org/10.1016/j.chemosphere.2021.130616
139. D.Yang, Y.Wang, J.Zhao, J.Dai, Y.Yan, L.Chen, J.Ye. *J. Colloid Interface Sci.*, **639**, 355 (2023); https://doi.org/10.1016/j.jcis.2023.02.060
140. Z.Zhou, J.Li, L.Yang, M.Li, X.Ji, Y.Wang, Z.Gu. *Top. Curr. Chem.*, **384**, 7 (2026); https://doi.org/10.1007/s41061-026-00539-x
141. V.U.Pandit, P.M.Patil, G.Goncalves, M.Gupta, K.P.Hazarika, D.J.Late. *Chem. Phys. Rev.*, **7**, 011309 (2026); https://doi.org/10.1063/5.0301736
142. F.Messina, L.Sciortino, R.Popescu, A.M.Venezia, A.Sciortino, G.Buscarino, S.Agnello,R.Schneider, D.Gerthsen, M.Cannas, F.M.Gelardi, *J. Mater. Chem. C*, **4**, 2598 (2016); https://doi.org/10.1039/c5tc04096e
143. A.Sciortino, N.Mauro, G.Buscarino, L.Sciortino, R.Popescu, R.Schneider, G.Ciammona, D.Gerthsen, F.Messina. *Chem. Mater.*, **30**, 1695 (2018); https://doi.org/10.1021/acs.chemmater.7b05178
144. M.Gazzetto, A.Sciortino, M.Nazari, E.Rohwer, G.Giammona, N.Mauro, T.Feurer, F.Messina, A.Cannizzo. *ACS Appl. Nano Mater.*, **3**, 6925 (2020); https://doi.org/10.1021/acsanm.0c01259